UNIVERSIDADE DE LISBOA

FACULDADE DE CIÊNCIAS

DEPARTAMENTO DE FÍSICA

Generation and Characterization of a *Cerl2*-KO Embryonic Stem Cell Line

Ana Mafalda Alves Costa e Silva

Mestrado Integrado em Engenharia Biomédica e Biofísica
Perfil Engenharia Clínica e Instrumentação Médica

Dissertação Orientada por:

Prof. Dr. José António H. Belo, *Stem Cells and Development*, *Chronic Diseases Research Center* (CEDOC), Faculdade de Ciências Médicas da Universidade Nova de Lisboa

Prof. Dr. Hugo Alexandre Ferreira, Instituto de Biofísica e Engenharia Biomédica, Departamento de Física da Faculdade de Ciências, Universidade de Lisboa

2017

“Imagination is more important than knowledge.
Knowledge is limited. Imagination encircles the world.”

Albert Einstein

Acknowledgements

Firstly, I would like to thank Professor José Belo for accepting me in his team and for the opportunity to develop this fantastic and ambitious project. Also, for all the support, guidance and important discussions during the last year. I would like to thank Professor Hugo Ferreira for the relevant comments to the written work.

A very special thanks for José Inácio for all the patience and willingness to teach me the experimental techniques and for the motivation given in the first months that demonstrated to be frustrating until the first positive results appeared. Still, for all the revisions and comments given during the writing of this Dissertation.

To the other members of the team: Fernando Cristo, Oriol Bover, Graça Rosas, Sara Marques and Fernando Bonet thanks for having received me so well and for all the help given every time that I needed.

I am especially and eternally grateful to my Parents for all the support during the last few years and, mainly, for never ceasing to believe that I would achieve my dreams even the craziest. With them I learned that dreaming has no limits or barriers but only with work, dedication and love, dreams become memorable experiences.

Resumo

Até aos dias de hoje, a Embriogénese é considerada um dos mecanismos mais fascinantes e complexos de decifrar. Os processos que medeiam a origem, desenvolvimento e especialização de um oócito até este formar um organismo completo são exaustivamente estudados de forma a entender a origem das doenças congénitas.

Nos vertebrados, o coração é o primeiro órgão a ser formado tendo a funcionalidade de bombear o sangue e, desta forma, suprimir as constantes necessidades nutritivas do embrião. Por detrás da sua formação, várias vias de sinalização moleculares necessitam de estar intimamente relacionadas entre si. A mais pequena alteração numa delas leva ao surgimento de doenças cardíacas congénitas, afetando desde à nascença a qualidade de vida do Ser vivo. Deste modo, é crucial que sejam decifrados os mecanismos e moléculas por detrás da origem destas doenças, culminando na descoberta de terapias específicas bem como na sua prevenção.

Durante o desenvolvimento embrionário, são vários os mecanismos que determinam o correto posicionamento do coração através da origem sequenciada dos três eixos principais: o Anterior-Posterior (A-P), o Dorso-Ventral (D-V) e o Esquerdo-Direito (E-D). Este último, está implicado na definição do posicionamento do coração na caixa torácica, na sua rotação final bem como na correta morfologia dos ventrículos e aurículas. Uma das principais vias de sinalização que inicialmente medeia a diferenciação da mesoderme e o estabelecimento do eixo E-D é a via Nodal, integrante da família TGF-β composta por vários outros membros também fatores de crescimento. No ratinho, nas etapas iniciais, as proteínas Nodal deslocam-se assimetricamente para o lado esquerdo do nó, uma estrutura embrionária transiente, e aí interagem com várias proteínas antagonistas capazes de direcionar o seu fluxo para a Placa Lateral Esquerda da Mesoderme. Quando se verifica uma mutação em algum dos genes codificadores destas proteínas antagonistas do Nodal, a indução da sua cascata de sinalização é rapidamente afetada resultando em defeitos de lateralidade dos órgãos, nomeadamente do coração e das suas artérias.

Nas últimas décadas, vários modelos animais e celulares têm sido usados para mimetizar o fenótipo e genótipo característico de algumas patologias cardíacas humanas resultantes de anomalias de lateralidade. Nomeadamente, ratinhos *knockout* para o gene *Cerberus-like 2* (*Cerl2)* foram anteriormente desenvolvidos de forma a estudar as implicações por detrás da perda de função deste gene. Este mesmo gene é expresso assimetricamente no lado direito do nó, codificando a proteína Cerl2 identificada como uma relevante antagonista da via de sinalização Nodal. Aquando a ausência da sua atividade antagonista, verifica-se uma anormal ativação da sinalização Nodal também na Placa Lateral Direita da Mesoderme. Tendo em conta as suas funções moleculares, seria de esperar que os ratinhos mutantes apresentassem fenótipos de lateralidade anormal. Deste modo, foram descritos defeitos na orientação do eixo cardíaco (*looping* randomizado), falhas na formação do septo ventricular e auricular, transposição das grandes artérias, hipertrofia ventricular, entre outros. Ainda, verificou-se uma taxa de morte neonatal considerável, no primeiro dia após o nascimento, tendo sido estabelecida uma relação direta entre a perda de função deste gene e o fenótipo mortal nestes ratinhos. No entanto, entre a população de ratinhos *knockout* foram identificadas ligeiras diferenças nos fenótipos apresentados, sendo alguns livres de malformações no estabelecimento do eixo E-D.

Posteriormente, estudos de eletrocardiografia realizados a embriões e ratinhos neonatais *Cerl2*$^{-/-}$ permitiram estudar a eletrofisiologia e morfologia dos seus corações. De forma a ser independentemente

estudado o mecanismo de ação molecular do *Cerl2*, foram considerados apenas ratinhos sem fenótipo anormal de lateralidade. Os resultados revelaram um aumento do índice de massa ventricular esquerda, uma redução do pico de velocidade da artéria pulmonar e uma diminuição do ritmo cardíaco, comparativamente com a população *wild-type*. Com o intuito de desvendar o papel deste gene, foram realizadas análises histológicas a amostras de corações em diversas fases de desenvolvimento embrionário e fetal. O estudo revelou um aumento significativo da espessura do miocárdio constituinte do ventrículo esquerdo demonstrando ainda que este fenómeno se deve a hiperplasia dos cardiomiócitos, com um aumento associado do número de eventos mitóticos. Verificou-se, ainda, um aumento dos níveis de fosforilação Smad2 sugerindo que a via de sinalização Nodal/Activin/Smad2 poderá estar super estimulada na ausência de proteínas Cerl2. Salientando, esta via de sinalização foi identificada como uma das principais reguladoras do processo de cardiogénese.

No presente projeto, com o objetivo de analisar o papel do Cerl2 no processo de cardiomiogénese, células estaminais embrionárias foram derivadas de blastocistos dos ratinhos *knockout*. Foram usados os protocolos chave para a confirmação da estabilidade e propriedades de pluripotência das células geradas, podendo posteriormente ser usadas como um modelo de doença fiável. Análises ao cariótipo demonstraram que as linhas celulares derivadas apresentam estabilidade cromossómica, tanto a nível numérico como estrutural. Ao recorrer à técnica de imunofluorescência as células Estaminais Embrionárias revelaram marcação positiva para os marcadores NANOG, OCT4 e SSEA1 indicando a existência de expressão proteica dos mesmos. Corroborando estes resultados, níveis de expressão génica positivos foram identificados através da técnica de PCR quantitativo em tempo real (RT-PCR). Assim, foram amplificadas de forma significativa, amostras da sequência genética de *Nanog*, *Oct4* e *Sox2*, revelando uma vez mais a existência de propriedades de pluripotência. De forma a demonstrar a capacidade de diferenciação em todas as linhagens celulares que compõem um organismo, procedeu-se à diferenciação espontânea das células Estaminais Embrionárias *Cerl2*$^{-/-}$ através do método de cultura de Corpos Embrióides (EBs). Recorrendo uma vez mais a testes de imunofluorescência, verificou-se a capacidade de diferenciação nas três camadas germinativas – endoderme, mesoderme e ectoderme – através da presença de marcadores proteicos específicos para cada uma delas.

Usando o protocolo de diferenciação cardíaca por EBs, testou-se a hipótese de nas células estaminais *Cerl2*$^{-/-}$ a capacidade de diferenciação na mesoderme estar aumentada, comparativamente com células estaminais controlo (linha comercial E14). Observou-se um aumento substancial da capacidade de adesão, às placas de cultura, dos EBs derivados da linha mutante. Constatou-se, o surgimento de regiões com atividade cardíaca nos EBs *knockout* a partir do dia 6 de diferenciação, enquanto nos EBs derivados da linha *wild-type* estas regiões com contratilidade cardíaca apenas eram visíveis a partir dos dias 7 ou 8 de diferenciação. Durante este processo, foram contabilizadas as áreas de contratilidade verificando-se que, em média, no dia 10 do protocolo de diferenciação, cada EB *knockout* continha o dobro do número de áreas comparativamente com um EB da linha controlo. Estudando as variações temporais da expressão de genes característicos das várias etapas de diferenciação desde a mesoderme até à formação de cardiomiócitos maduros, através de RT-PCR, verificou-se um aumento da expressão de *Mesp-1*, *Isl1* e *Nkx2.5* indicando um incremento no número de células progenitoras cardíacas geradas. Analisando os níveis de expressão de genes implicados na maturação dos cardiomiócitos, verificou-se um aumento da regulação de *α-MHC* e uma diminuição na regulação de *cTnT* nas células diferenciadas *Cerl2*$^{-/-}$. Conclui-se que as células KO têm uma maior capacidade de diferenciação mesodérmica, levando à produção de um maior número de progenitores cardíacos e, consequentemente, a um aumento no número de cardiomiócitos gerados. No entanto, estes aparentam ter uma maturação incompleta.

Em conclusão, os resultados desenvolvidos neste projeto possibilitaram o estabelecimento e caracterização de linhas estaminais *Cerl2*$^{-/-}$ de ratinho servindo estas como um modelo para estudar as patologias congénitas relacionadas com este gene. Foram reveladas as primeiras descobertas sobre as

alterações nos mecanismos de cardiomiogénese resultantes da perda de função do gene *Cerl2*. Futuramente, poderão ser usadas como ferramenta para a descoberta de novos mecanismos biológicos das proteínas Cerl2 ou mesmo até para o desenvolvimento de terapias celulares.

Palavras-Chave: *Cerl2*, eixo Esquerdo-Direito, células Estaminais Embrionárias, diferenciação em cardiomiócitos.

Abstract

Embryogenesis is a well-organized process capable of originating the complex mammalian organisms. Even a slight change in the signaling pathways is capable of significantly altering the biological mechanisms leading to a mutant phenotype. The heart is the first organ to be formed during this process, according to its vital functions since the first days of an embryo's life throughout the entire life of the mammalian organism. Sporadically, cardiogenesis does not occur with the normal coordination and some signaling pathways are altered resulting in congenital heart diseases. Thus, it is crucial to uncover the molecular and morphogenetic mechanisms that lead to these pathologies in order to discover new therapies' insights and provide genetic prevention.

A *Cerberus/Dan* family member, the mouse *Cerberus-like 2* (*Cerl2*) gene, has been studied and identified as a *Nodal* antagonist, capable of interfering in the most relevant steps during Left-Right (L-R) axis establishment that lead to the asymmetric patterning of the heart. Its function consists to spatially regulate Nodal proteins to the Left Lateral Plate Mesoderm, at the embryonic stage of development. In *Cerl2* knockout mice, it was reported a wide range of laterality defects with associated cardiac failure and significant death rate on the first day after birth. Previously, a massive increase of the ventricle walls was observed as a consequence of cardiomyocytes' hyperplasia, verified by an increase in their mitotic index.

In order to uncover the possible roles of Cerl2 in the regulation of the signaling pathways underlying cardiomyocyte proliferation and differentiation, three *Cerl2*$^{-/-}$ Embryonic Stem cell (ES cell) lines were derived from blastocysts of the mutant mice. Using this disease model, it was possible to begin the study of the implications of Cerl2 in the spatiotemporal control of cardiac progenitors' proliferation and its differentiation into mature cardiomyocytes. Firstly, the normal chromosomic number and structural stability of the derived lines was confirmed by G-banding staining. Then, pluripotency properties were verified using standard protocols, such as immunofluorescence microscopy that demonstrate positive protein expression for NANOG, OCT4 and SSEA1 markers. Also, through real-time amplification of endogenous RNA expression for *Nanog*, *Oct4* and *Sox2* genes it was confirmed the presence of pluripotency properties. In order to prove the differentiation capacity in the three germ layers, the ES cells were spontaneously differentiated and positive protein expression for endoderm, mesoderm and ectoderm was confirmed through immunostaining.

Using the Embryoid Bodies culture, the *Cerl2*$^{-/-}$ ES cells were differentiated into cardiac cells. It was notorious a significant change in the number of produced beating foci areas compared to the control line: the knockout cells originated the double of the cardiac foci compared to the wild type cells, even at day 10 of the differentiation protocol. Using the real-time PCR technique, the levels of early cardiac genes expression were studied, showing a statistical upregulation of *Mesp-1*, *Nkx2.5* and *Isl1* genes in the differentiated *Cerl2*$^{-/-}$ cells. Also, the expression of mature cardiac markers was evaluated resulting in increased levels of *α-MHC* and reduced levels of *cTnT* in these cells. Concluding, loss-of-function of *Cerl2* leads to a possible increase in the cardiac progenitor cells resulting in a higher number of derived cardiomyocytes. However, despite of showing early beating actions they did not reveal a complete maturation.

Ultimately, the present project uncovers the first insights in the *Cerl2* role during mouse cardiomyogenesis, mainly in the specification of the number of cardiomyocytes that will populate the mature myocardium.

Keywords: *Cerl2*, Left-Right axis, Embryonic Stem cells, cardiomyocytes' differentiation.

Contents

List of Tables

List of Figures

Abbreviations

Afp	Alpha Fetoprotein
α-MHC	*Alpha Myosin Heavy Chain*
A-P	Anterior-Posterior
AVE	Anterior Visceral Endoderm
BMP	Bone Morphogenetic Protein
cDNA	Complementary Deoxyribonucleic Acid
Cerl2	*Cerberus-like 2*
CMC	Cardiogenic Mesodermal Cells
cTnT	*Cardiac Troponin T*
DMEM	Dulbecco's Modified Eagle Medium
DMSO	Dimethyl Sulfoxide
DNA	Deoxyribonucleic Acid
dNTP	Deoxynucleotide
D-V	Dorso-Ventral
DVE	Distal Visceral Endoderm
E	Embryonic Day
EB	Embryoid Body
EGF-CFC	Epidermal Growth Factor-cripto, frl-1, cryptic
ES	Embryonic Stem
FBS	Fetal Bovine Serum
FGF	Fibroblast Growth Factor
FHF	First Heart Field
Fwd	Forward
Gapdh	*Glyceraldehyde-3-Phosphate Dehydrogenase*
Gdf1	*Growth/ Differentiation Factor 1*
GSK3	Glycogen Synthase Kinase 3
ICM	Inner Cell Mass
IgG	Immunoglobulin G
Isl1	*Isl1 Transcription Factor, LIM Homeobox 1*
KO	Knockout

LIF	Leukemia Inhibitor Factor
LPM	Lateral Plate Mesoderm
L-R	Left-Right
MEF	Mouse Embryonic Fibroblast
Mesp-1	*Mesoderm Posterior 1*
NEAA	Non-Essential Amino Acids
Nkx2.5	*NK2 Homeobox 5*
NOD	Non-Obese Diabetic
Oct4	*Octamer 4*
OFT	Outflow Tract
PBS	Phosphate-Buffered Saline
PCR	Polymerase Chain Reaction
PFA	Paraformaldehyde
Pitx2	*Paired-like Homeodomain Transcription Factor 2*
PrE	Primitive Endoderm
PS	Primitive Streak
qRT-PCR	Quantitative Real-Time Polymerase Chain Reaction
RNA	Ribonucleic Acid
Rv	Reverse
SHF	Second Heart Field
Sox2	*SRY-Related High Mobility Group Box 2*
Sry	*Sex-determining Region Y*
SSEA-1	*Stage-Specific Embryonic Antigen-1*
Stat3	Signal Transducer and Activator of Transcription 3
TAE	Tris-Acetate-EDTA
TE	Trophectoderm
TGF-β	Transforming Growth Factor β
UV	Ultraviolet
Wnt	Wingless/ Integrated Family Members
WT	Wild Type

Chemical Symbols

$CaCl_2.2H_2O$	Calcium Chloride Dihydrate
CO_2	Carbon Dioxide
$MgCl_2.6H_2O$	Magnesium Chloride Hexahydrate
NaCl	Sodium Chloride
KCl	Potassium Chloride

Units

%	Percentage
µg	Microgram
µg/mL	Microgram per Milliliter
µL	Microliter
µM	Micromolar
bp	Base Pair
ºC	Degree Celsius
kb	Kilobase Pair
mL	Milliliter
mM	Milimolar
ng	Nanogram
pH	Potential of Hydrogen
rpm	Rotations per Minute
U/µL	Units/Microliter
V	Volt
v/v %	Volume/ Volume Percentage
xg	Times Gravity
w/v %	Weight/ Volume Percentage

1. Introduction

In the last decades, cardiovascular diseases have become the first cause of morbidity and mortality, in developed countries, adversely affecting the patients' quality of life (Naghavi et al., 2015). Just in Europe, more than 4 million of people die every year mainly due to ischaemic heart disease and congestive heart failure (Townsend et al., 2016). Unfortunately, still nowadays, scientific data indicate that regeneration capacity in human heart is limited, and the only body response for these conditions consist in an inflammatory process, originating a non-contractile scar (Coulombe et al., 2014) (Czubryt, 2012). Consequently, myocardium tissue is permanently damaged caused by a dysfunctional remodel tissue leading to the loss of cardiomyocytes' number and decrease of their function with associated electrophysiological instability (Braunwald & Pfeffer, 1991).

According to the available therapies, the pharmacologic solutions and mechanical support advices, could not allow the functional regeneration of cardiomyocytes and they did not offer a positive long-term solution in the majority of the patients. So, heart transplantation is still the only definitive treatment for heart failure despite of its associated complications.

In the last two decades, a lot of effort has been done to develop an efficient protocol to derive cardiomyocytes from pluripotent and multipotent stem cells with the purpose to recover the function of patients' cardiomyocytes (Le et al., 2017). The possibility that these two cell lineages could induce differentiation and repopulation of new cardiac precursor cells or cardiomyocytes in the damaged myocardium allowed to start testing these protocols in human patients. The adult bone marrow-derived cells have been used in the majority of the cell-therapy trials because of the high number of obtained cells as well as the safety and feasibility of its use (Cambria et al., 2016). Attending to meta-analysis studies, considering more than 2600 patients, this cell-based therapy improves around 3.96% of the left ventricular ejection fraction with a reduction in the size of infarct scar, as well as exercise capacity improvement (Jeevanantham et al., 2012) (Fisher et al., 2015). Another promising therapy approach uses the potential of the cardiac progenitor cells' population, present in postnatal mouse and human hearts, to promote cardiomyocytes differentiation. By the emerging of controversial evidences showing that the human heart repairs about 1% per year, this type of cells have been used in the attempt to stimulate this low natural renewal rate (Bergmann et al., 2009) (Bergmann et al., 2015). However, this regeneration potential declines with age and it is not sufficient to promote myocardium replacement after an injury, so the next milestone consisted in the first clinical attempt to infuse the c-kit^{+} population of cardiac stem cells in patients suffering with ischemic cardiomyopathy (Bergmann et al., 2009) (Bolli et al., 2011). This phase I trial, denominated SCIPIO – Cardiac Stem Cell Infusion in Patients with Ischemic Cardiomyopathy – , showed significant improvements in the left ventricular ejection fraction and reduction in size of the infarct scar tissue after several months from the infusion of autologous cells expanded *in vitro* (Bolli et al., 2011) (Chugh et al., 2012). Other phase I trials appeared in the same year (e.g., CADUCEUS and ALCADIA), demonstrating relevant clues about the safety and feasibility of the use of injection of autologous cardiac stem cells (Yacoub & Terrovitis, 2013). Despite of the promising results, these cardiac repair therapies have been under an exhaustive scrutiny related to their efficacy in the promise of long-awaited myocardium regeneration. Still, there is a long journey until their outcomes could strongly influence the use of stem cells in the currently medical practice for myocardium renewal.

Until then, clinical trials with larger number of patients and a longer time follow up of the treatment need to be carry out.

In meantime, Embryonic Stem cells have been widely used as an *in vitro* model to uncover mechanisms and signaling pathways involved during mouse and human early cardiomyogenesis (Habib et al., 2008) (Dambrot et al., 2011). They have been demonstrated to be a useful model because of the excellent abilities to mimic the most relevant mechanisms that occur *in vivo* during embryogenesis. Thus, the *Cerberus-like 2* (*Cerl2*) gene has been studied because of its implication on critical mechanisms during mouse embryonic heart development. Its role is crucial for an appropriate asymmetric positioning of the organs and a correct development of them, especially the heart (Marques et al., 2004). In humans, the homologous gene is denominated *DAND5*. It is medical documented that a loss of asymmetry is implicated in several human diseases, such as heterotaxia syndrome and congenital heart disease (Ramsdell, 2005). So, a recent study started to link these diseases with the *DAND5* abnormal expression in patients culminating in new molecular insights and classifying this gene as a determinant candidate for the referred congenital heart defects (Cristo et al., 2017).

Recent data show that a loss of function of *Cerl2*, in knockout mice, leads to massive increase of ventricular walls being a consequence of an increase in mitotic index of the cardiomyocytes (Araújo et al., 2014). Also, this increasing proliferation in these mutant mice was associated with extension of TGF-β/Nodal/Wnt signaling in heart, being these signaling pathways well known to be involved in cardiac differentiation and proliferation (Araújo et al., 2014) (Parikh et al., 2015). In this way, it is reasonable to hypothesize that Cerl2 proteins control both signaling pathways in the mouse heart by being a master regulator of them during embryogenesis. This leads to the possibility of secreted Cerl2 proteins are involved in the mechanism responsible for the cardiomyocytes proliferation and, probably, be involved in the decision mechanism of the number of originated cells.

1.1 Aims of the Project

To improve the cell-based therapies for myocardium repair in currently clinical progress, it is firstly necessary to clearly understand the molecular mechanisms and signaling pathways involved behind cardiomyogenesis. Also, several disease models are created in the laboratory environment as a tool to study the molecular and genetic mechanisms that lead to pathogenesis of cardiac human diseases with the ultimate propose to find new therapeutics. Along the years, the mouse has been used as a preferred animal model to mimic cardiac human diseases taking the advantage of the physiologic and genetic similarities between these two species. So, knockout mutant mice are routinely produced in order to investigators obtain a model for study the loss-of-function genes.

According to these information, *Cerl2* knockout mice had already been produced and their abnormal phenotype was quite studied by echocardiography and morphogenetic experiments. The obtained results led to the emergence of several important questions. Does Cerl2 proteins control TGF-β and Wnt pathways during heart development? If Cerl2 is responsible for the dual regulation of these signaling pathways, could be possible to improve cardiomyocyte proliferation? Also, does the loss-of-function of *Cerl2* gene change the number of differentiated cardiomyocytes?

To answer these questions, the first objective of the present Dissertation consists in deriving a *Cerl2* knockout mouse Embryonic Stem cell line. Using this *in vitro* model of congenital heart disease, it will be possible to examine the mechanism underlying of Cerl2 role and discover how it could modulates the signaling cascades involved in the inducing of cardiomyocyte proliferation. Then, using the derived line, the others main objectives will consist in:

(i) Determine if proliferation capacity is increased in the *Cerl2* knockout Embryonic Stem cell-derived cardiomyocytes comparing with a control line;
(ii) Determine how targeting *Cerl2* function could be translated in production of a high number of cardiomyocytes that could be, posteriorly, used for regenerative medicine;
(iii) Address the fundamental roles of *Cerl2* during cardiomyocyte differentiation process, mainly related to TGF-β and Wnt pathways.

1.2 Organization of the Thesis

The present dissertation is organized in five Chapters. Firstly, the present Chapter exposes the contextualization of the cardiovascular disease problem, the offered solutions of treatment with its inherent limitations and a brief introduction of the main process in which the *Cerl2* gene is involved, culminating in the main motivations and objectives of this Dissertation.

Chapter 2 provides essential background information related with early mouse development and the mechanisms behind heart embryology. Some studies and results related to the most important genes involved in cardiogenesis signaling pathways are described for a clearly understanding and correlation of the role of *Cerl2*. To complement this introductory knowledge, this Chapter will also contain the state-of-art of Embryonic Stem cells field, focusing in the main steps of generation and maintenance of these cells from the first successfully attempt until the relevant recent achievements. At the end of this Chapter, the significance of a *Cerl2* knockout Embryonic Stem cell line will clearly be understood as a tool for cardiac disease models in order to study its embryonic roles during cardiogenesis.

In Chapter 3 the methods and materials used during the entire project are exposed in detail. Also, commercial references of the reagents are indicated.

In Chapter 4, the results obtained from all the experiments are presented as well as discussion allied with some important steps performed to reach them.

Finally, the Chapter 5 is composed of the conclusions and suggestions for future work that could complement the knowledge developed so far.

2. Background

2.1 Early Mouse Development

The journey of mouse embryogenesis starts with a fertilized cell, the zygote, that consist in a totipotent cell capable to subsequently divide in smaller ones – the blastomeres. After several mitotic divisions, through a compaction process, the morula is capable to generate the blastocyst that is composed by two different cell lineages, the trophectoderm (TE) and the inner cell mass (ICM) (Figure 2.1) (Johnson & Ziomek, 1981). It is known that the first contact of the embryo with the maternal uterine walls is due to the TE, also giving rise to specific tissues in placenta, and the ICM is mainly involved in the embryo formation, by a cell population that will form the pluripotent epiblast (Marikawa & Alarcón, 2009). Then, at Embryonic day 3.75 (E3.75), the ICM differentiates into the epiblast and the primitive endoderm (PrE). Studies using lineage-tracing of mouse embryos revealed that upregulation of *Cdx2* gene is necessary for the proliferation of TE cells' population while *Nanog* and *Oct3/4* participate in the early cell fate of ICM cells (Morris et al., 2010) (Niwa et al., 2005). Thus, the epiblast gives rise to the entire embryo as well as some extraembryonic structures through its pluripotency properties. On the other hand, the PrE cells are known to contribute to the distal visceral endoderm (DVE) formation, originating later the anterior visceral endoderm (AVE) (Takaoka & Hamada, 2012). At this stage, for a correct establishment of the primitive Anterior-Posterior (A-P) axis, it is crucial the positive expression of the Nodal antagonists *Lefty1* and *Cer1* in the DVE cells (Takaoka et al., 2011).

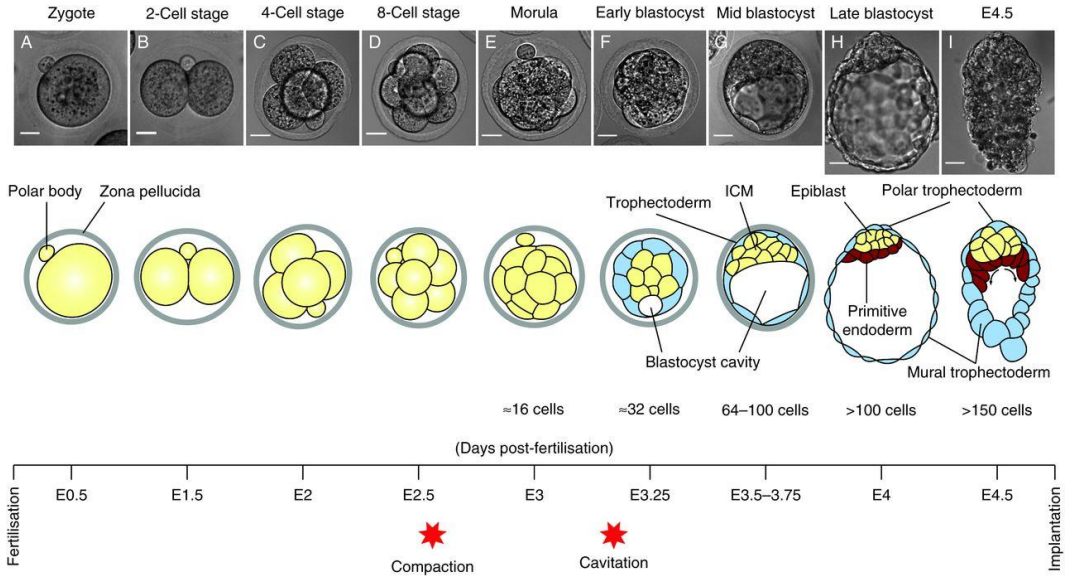

Figure 2.1: Overview of the early mouse development. The zygote consists in a totipotent cell capable of subsequently dividing in smaller cells called blastomeres, until the morula stage its reached. At E3.5, the blastocyst is composed by two different cell lineages: the inner cell mass (ICM) and the trophectoderm (TE). Ultimately, the ICM is responsible for the embryo formation (figure taken from http://www.devbio.biology.gatech.edu/?page_id=8796, consulted on 8th October 2016).

2.2 The Establishment of the Three Embryonic Body Axes

2.2.1 The Anterior-Posterior and the Dorso-Ventral Axes

During the gastrulation, the morphogenesis of the mouse embryo takes place leading to the formation of the three germ layers – ectoderm, mesoderm and endoderm – that give rises to all type of tissues and ultimately to the generation of a three-dimensional body plan (Tam & Behringer, 1997). At the beginning of this process, around E6.0, the epiblast cells undergo a transition to form mesoderm and, in the meantime, they generate the primitive streak (PS), that consists in a transient embryonic structure (Figure 2.2). The migration of these epiblast derived cells to the opposite side of AVE zone results in the PS located at the posterior side of the embryo, being this stage the morphologic landmark of the A-P axis determination (Tam & Behringer, 1997). The PS, in its late stage, contributes to the formation of the node, described above, with organizer roles implicated in derivation of the primitive mesodermal structures and the notochord (Davidson & Tam, 2000). The notochord is involved in the specify of the neurons from the neural tube and in the mouse somites formation. These last ones represent transient segments of the embryo formed prior of body formation step (Pourquié, 2003). Ultimately, the time line formation of the dorso-ventral (D-V) axis is characterized by the node generation (Beddington & Robertson, 1999).

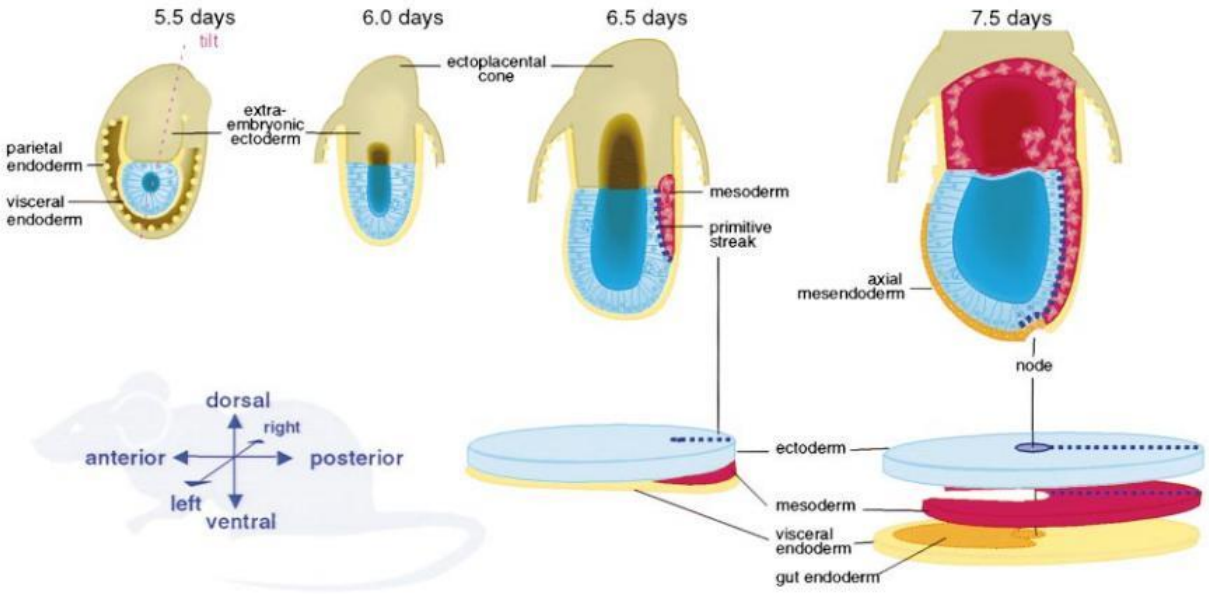

Figure 2.2: The establishment of Anterior-Posterior (A-P) and Dorso-Ventral (D-V) body axes during mouse gastrulation. The diagram shows the temporal formation of the PS and the morphologic changes involved in the establishment of the A-P and D-V body axis (figure modified from Beddington & Robertson, 1999).

2.2.2 The Left-Right Axis

The determination of Left-Right (L-R) axis, in early mouse embryos, was firstly associated to the node region described as a concave triangular zone located at the ventral midline surface of the embryo and formed during the gastrulation (Figure 2.2) (Harvey, 2010). Nodal flow is involved in three main processes beyond L-R asymmetry. Around E7.5, an asymmetric signal generated in the mouse node, by motile cilia, suffers a leftward flow alteration towards the left side of the lateral plate mesoderm (LPM), consisting in the first step of the symmetry-breaking event (Shiratori & Hamada, 2006). Allied to this, Cerl2 proteins are capable to directly bind to Nodal and regulate its asymmetric expression by restricting

it to the left LPM (Marques et al., 2004). When an asymmetric *Nodal* expression starts to occur in left LPM's cells, the second step of the L-R axis patterning is stablished (Shiratori & Hamada, 2006). However, the exact mechanism beyond this molecular signaling migration still remains unclear.

The L-R asymmetric morphogenesis of visceral organs completes the third step beyond this axis patterning. During this step, *Pitx2* acts as a master regulator gene in a conserved and altered activity patterning in some species. In order for this process to be triggered, the asymmetric expression of *Pitx2* needs to be initiated in the left LPM (Shiratori & Hamada, 2006). This *Nodal* target gene is described as a bicoid-type homeobox transcription factor and its known to act as a downstream of Nodal proteins (Yoshioka et al., 1998) (Ryan et al., 1998) (Piedra et al., 1998) (Logan et al., 1998). Moreover, anomalies in the L-R axis establishment leads, in most cases, to laterality defects known as *situs inversus*, *isomerism* and heterotaxia, which will be discussed below. Still, combining these knowledge, some studies of patients suffering with congenital laterality defects indicate that Nodal signaling is potentially extended to human. Also, some of these human mutations are related to the loss-of-function of proteins that interact with Nodal. For example, human mutations in the *LEFTY* genes, homologous to *Lefty1* and *Lefty 2* in the mouse, were found in patients with associated L-R axis malformation, mainly left pulmonary *isomerism* and cardiac malformations (Kosaki et al., 1999). Also, patients showing an abnormal phenotype characterized by tetralogy of Fallot and transposition of the great arteries demonstrated to have a heterozygous mutation in the *GDF1* gene (Karkera et al., 2007).

2.2.2.1 The Nodal Signaling

Nodal is a member of the Transforming Growth Factor type β (TGF-β) superfamily of secreted signaling factors, playing essential roles during embryogenesis mainly the mesoderm and endoderm induction, as well as in specification of the primary body axes, as explained before (Kawasumi et al., 2011). Previous study, using mouse *Nodal* mutants, showed the absence of PS formation in these animals leading to a sporadic development of some posterior mesoderm and its randomly position (Conlon et al., 1994).

Several molecules, also included in the TGF-β superfamily, have been implicated in the mechanisms of the Nodal signaling pathway that are mainly involved in the process of a successful L/R axis establishment. Two of them are the *Lefty* genes that, despite of being integrated in the TGF-β superfamily, present a different structure compared to the other molecules. During the nodal flow, *Lefty1* and *Lefty2* show the capacity to act as spatial and temporal antagonists, preventing excessive Nodal expression and blocking its migration to the right LPM, through a negative feedback loop (Meno et al., 2001) (Hamada et al., 2001). In parallel with this, the *Gdf1* gene starts to be expressed in the mouse node. It is thought that the Gdf1 is directly involved in transferring its signal from the node to the LPM interacting, in this way, with Nodal proteins. This could be explained according to the inexistence of asymmetric Nodal expression in the LPM and presence of right isomerism saw in *Gdf1*$^{-/-}$ mice (Rankin et al., 2000).

On the other hand, the *EGF-CFC* gene family encodes proteins that act as competence factors recruited during Nodal signaling in various species as Xenopus, zebrafish, mouse and humans. These extracellular proteins are composed by an altered epidermal growth factor (EGF)-like motif and a cysteine-rich (CFC) domain (Salomon et al., 2000). Data demonstrate that function of cripto proteins, comprised in this family, have similarities with Nodal proteins. Using tracing studies with mutant crypto mice, the resulted abnormal phenotype was characterized by absence of PS formation and therefore defects on embryonic mesoderm suggestive of loss of Nodal proteins (Ding et al., 1998). These findings are explained by posterior data showing that, when Nodal receptors bind to the EGF-CFC factors, its proteins are likely to specifically interact with Alk4 and ActRIIB activin receptors (Yeo & Whitman, 2001). When its

occur, Nodal signaling is activated and transduced by phosphorylation of Smad2/Smad3 in an intracellularly mechanism. Its association with Smad4 is known to originate transcriptional complexes that with association with FoxH1 transcription factor leads to expression regulation of some downstream Nodal target genes like *Lefty1/2* and *Pitx2* in the nuclear cells region (Figure 2.3) (Shen, 2007). Another important member of the Nodal signaling cascade, the Cerberus-like family, plays an essential role in order to maintain its signaling, specially through an antagonistic activity.

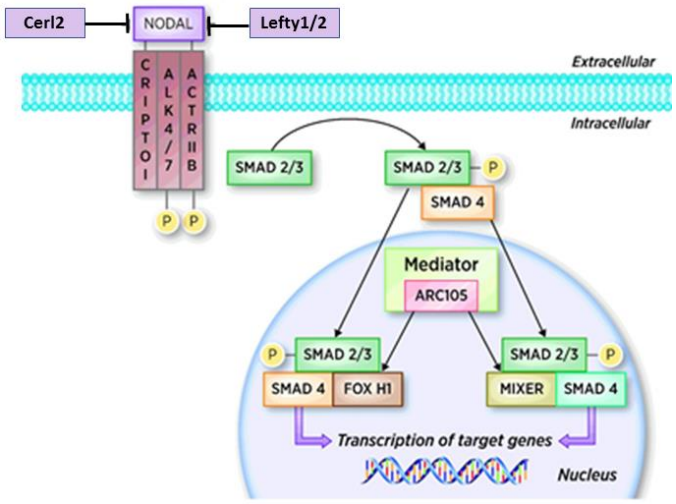

Figure 2.3: Nodal Signaling. Cerl2 and Lefty1/2 proteins interact with Nodal to regulate its levels and prevent its signaling migration to the incorrect side of the LPM (figure modified from Kalyan et al., 2017).

2.3 The Cerberus Family

The *Cerberus-like* (*Cer-l*) family is part of the cysteine-knot superfamily (Belo et al., 2009). It encodes for small secreted proteins – 272 a.a., Cerl-1 and Xcer, and 185 a.a., Cerl2 – that act as antagonists of Nodal, BMP and Wnt proteins (Marques et al., 2004). In terms of its protein domains, the Cer-l family is composed by 9 cysteines, where at the N-terminal a signal peptide is bind and at the C-terminal region a Cystein-Rich Domain (CRD) is formed (Belo et al., 2009).

The *Xenopus* embryos were the first animal model used to study *Cerberus* expression. Cer-l was initial identified in this species (Xcer), being this novel secreted protein expressed in the yolky anterior endomesoderm located in Spemann's organizer (Bouwmeester et al., 1996). Studies performed by injecting *Xcer* mRNA into blastomeres have resulted in formation of ectopic heads and duplicated internal organs, leading this phenotype to the designation of this gene (Bouwmeester et al., 1996). Besides the mentioned Cerberus-associated proteins for mouse (Cerl1 and Cerl2) and *Xenopus* (Xcer), others have been discovered in vertebrate species: the cCer in chicken, the zCharon in zebrafish and the Dand5 in humans.

2.3.1 Cerberus-like 2

Cerberus-like 2 (*Cerl2*) is a member of the *Cerberus/Dan* family, located on chromosome 8 in mouse, and was identified as a Nodal antagonist playing an important role in the L/R axis establishment during the mouse gastrulation (Marques et al., 2004). Studies showed that *Cerl2* encodes for a secreted 20-kDa protein, capable to directly bind to Nodal and, according to its small size, shows a dynamic localization on the node during early somitogenesis (Marques et al., 2004) (Inácio et al., 2013). Analysis to the *in vivo* subcellular localization of the Cerl2 protein demonstrated that, in early somite stage, its expression

is limited to both sides of node presented in perinodal crown cells (Inácio et al., 2013). However, the level of expression of Cerl2 in the right side of the node is notorious at 2-somite stage being dynamically transposed to the left side of the node at 3-4-somite stage (Inácio et al., 2013). After 6-somite stage, Cerl2 expression extinct in this location. According to these results, the hypothesis of Cerl2 be dependent of nodal flow was taking into account. And, the same study showed that both expression and localization of Cerl2 protein in the node is, indeed, dependent of nodal-flow signaling (Inácio et al., 2013).

2.4 Mouse Heart Development

The heart is the first organ to be formed during early development, immediately after gastrulation, being a master source of complexity and vital functions (Brand, 2003). Most of the cardiac progenitor cells are descendent from the mesoderm germ layer (Buckingham et al., 2005). The processes involved during this mesoderm derivation are primarily controlled by the Wnt, FGF and TGF-β families of signaling molecules (Später et al., 2014).

Early cardiogenesis starts with the migration of naïve cardiogenic mesoderm cells (CMCs) from the PS that will populate the splanchnic mesoderm layer located in the LPM region (Brade et al., 2013). Here, these heart cell precursors started to form a primitive heart structure called cardiac crescent (Figure 2.4). At E7.5 this structure is completely formed being a result of the first recruitment of CMCs-derived progenitors also commonly designated as first heart field (FHF) (Galdos et al., 2017). At the same time, the second heart field (SHF) progenitors, recruited from the pharyngeal mesoderm layer in the LPM, place medially and anteriorly to the FHF (Xin et al., 2013). By E8.0-E8.5, a primordial and linear heart tube is originated by the fusing of these FHF progenitors at the midline of the embryo, marking the start of beating function and acting as a scaffold to heart maturation (Nishii & Shibata, 2006). At this stage, cells migrated from the SHF lead to its elongation and expansion, in posteriorly and anteriorly regions, until give rise to arterial and venous poles (Meilhac et al., 2014). Then, the heart tube undergoes rightward looping mediated by L-R signaling information (Kathiriya & Srivastava, 2000). Ultimately, the SHF progenitors will derive to the outflow tract, right ventricle and both atria of developing heart while the FHF progenitors contribute to the left ventricle and atria (Figure 2.4) (Buckingham et al., 2005). The growing, differentiation and specialization steps lead to the correct positioning of the four cardiac chambers, at stage E10.5, continuing the complex process of heart maturation with septation and valve formation until E15.0 (Xin et al., 2013).

Despite of most of cells derived from FHF and SHF will turn on mature cardiomyocytes, these progenitor cell lineages also will give rise to other cell types that compose the mature heart and contribute to vessels composition: smooth muscle cells (SMCs), cardiac fibroblasts (CFs) and endothelial cells (Waldo et al., 2005) (Moretti et al., 2006).

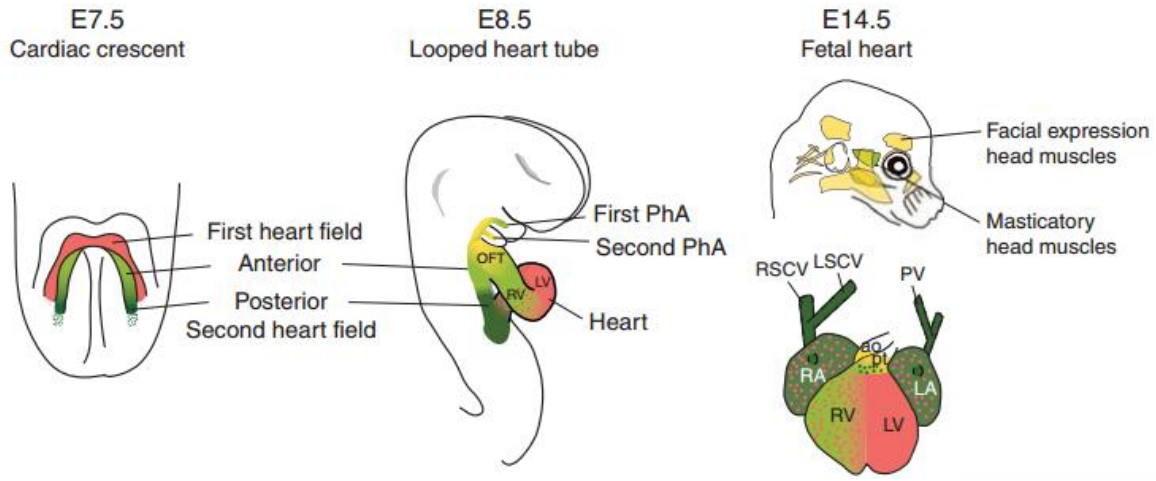

Figure 2.4: First (FHF) and second (SHF) heart fields formation and subsequent derivative tissues in mature heart and head in mouse. The FHF (red) and the SHF (green) are shown at different development stages during heart formation. The FHF progenitors will give rise to left ventricle (LV) and atria while SHF progenitors are involved in derivation of the outflow tract (OFT), right ventricle (RV) and atria. Also, some SHF progenitors are involved in formation of facial muscles of the head (figure modified from Meilhac et al., 2014)**.**

2.4.1 Failure in L/R Axis Leads to Laterality Defects

As described previously, a correct position of the internal organs is mainly due to the presence of an asymmetric signaling of the mentioned target genes of Nodal. When Nodal signaling undergoes a change or break in its temporal and spatial activation, regular organ's positioning is altered (Shiratori & Hamada, 2014). This medical condition is designed as laterality defects and, normally, its abnormal phenotype leads to a decrease in health conditions in humans (Shiraishi & Ichikawa, 2012). According to the most common types, laterality defects can be classified as: *situs inversus totalis* when a complete reversion of organs' symmetry occurs; heterotaxia when only some organs are reversed while others show a normal position (also designed as a partial *situs inversus*); and *isomerism* when organ's asymmetry is not present and can be divided in two types, the *left isomerism* when both sides become with left symmetry and *right isomerism* when both sides have a right symmetry (Figure 2.5) (Fujinaga, 1997).

The first abnormal signal of these phenotypes can be verified in the orientation of the cardiac loop, that shows an incorrect L-R axis positioning (Ramsdell, 2005). Since this deficiency is originated in the initial stages of cardiac embryogenesis, consequently several cardiac defects are also present in patients. The most typical ones are the atrioventricular septal defects, single atrium and right ventricle, aortic arch malformations and malposition of great arteries (Shiraishi & Ichikawa, 2012). In this way, laterality defects are commonly related with congenital heart diseases involving mutations in *NODAL* gene or any of its regulator genes.

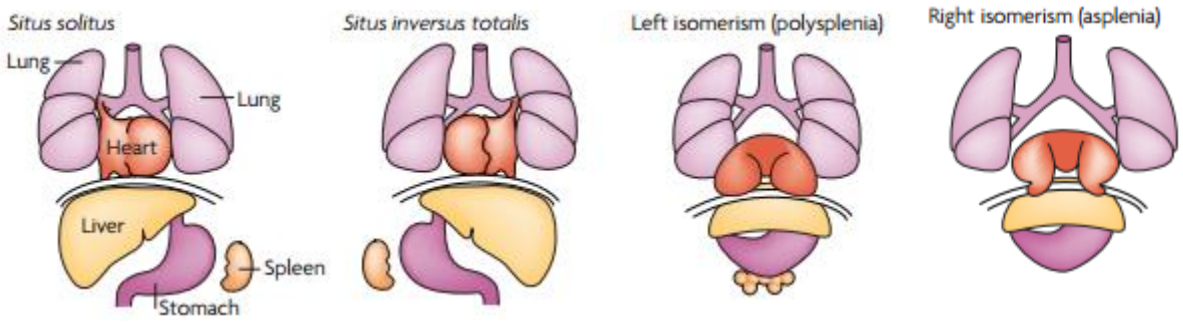

Figure 2.5: Morphological spectrum of laterality defects. The *situs solitus* consist in normal L-R body asymmetry. On the other hand, patients showing *situs inversus totalis* display a complete reversion of organs' symmetry. The *isomerisms* are a heterotaxia type, classified as *left isomerism* or *right isomerism* (figure modified from Fliegauf et al., 2007).

2.5 Mouse Embryonic Stem Cells

The Embryonic Stem (ES) cells are a very singular type of stem cells, derived from human or mouse embryos, characterized by their capacity to give rise to all the cell types of the three primordial germ layers. Using specific culture conditions, ES cells can be derived from the ICM of the mouse blastocyst maintain their unlimited or prolonged capacity to self-renew.

2.5.1 *In Vitro* Culture Conditions

Since the first successfully mouse ES cell line was derived from mouse blastocyst, various other ES cell lines have been derived and characterized in order to study the early mammalian development and used as disease models (Evans & Kaufman, 1981) (Martin, 1981). Inspired by previously studies of generation of teratocarcinoma cells, Evans and Kaufman as well as Martin, in independently investigations, established the basic principles to derive mouse ES cells, that consisted in coculture blastocysts with mouse embryonic fibroblast (MEF) cells using calf serum. With these culture conditions, they aimed to promote proliferation of ES cells colonies and retain an undifferentiated phenotype.

However, for many years, some ES cell lines were inefficiently derived or impossible to be produce from some mice strains. It became apparent, by some studies, that the facility and efficiency of ES cells derivation was dependent on the mice strain used; the 129 strain was determined as the most permissive while using others, like CBA and NOD strains, was not possible without a discovery of some molecules capable to overcame this experimental issue (Batlle-Morera et al., 2008) (Ying et al., 2008). Thus, a new stem cell culture system was reported bringing a huge step forward to solve this problem. This culture regime, called the "2i medium" is composed by two chemical kinase inhibitors, the CHIRON99021 and the PD0325901, capable to promote long-term self-renewal of mouse ES cells (Ying et al., 2008). There, by using the 2i condition medium, was possible to derive ES cells from strains previously impossible, including the NOD strain with satisfactory efficiency (Hanna et al., 2009) (Ying et al., 2008).The first one, the CHIRON99021, inhibits the glycogen synthase kinase 3 (GSK3), a central molecule modulator in Wnt signaling, stabilizing the cells proliferation by regulation of pluripotency and epigenetic factor (Ying et al., 2008). Prior study show that neural differentiation is repressed using this GSK3 inhibitor, consistent with the stemness maintaining resulted from Wnt activity (Aubert et al., 2002). The second, the PD0325901, is described as a MEK inhibitor, capable to block the Erk1/2 signaling (Ying et al., 2008). Recent study, reveal the main consequences of Erk activation in ES cells translated in endodermal lineage differentiation, mimetizing the PrE differentiation program *in vivo* (Hamilton & Brickman, 2014).

One of the *in vitro* critical conditions to initial sustain the efficiently derivation of ES cells consist in cocultured them with mitotically inactivated MEFs, denoted as feeder layers, since these cells have the ability to release important factors and increase the ES cells seeding and growing (Evans & Kaufman, 1981) (Martin, 1981). The most relevant one, the secreted leukemia inhibitor factor (LIF), is an important cytokine belonging to the interleukin 6 (Il-6) family, with the capacity to enable mouse ES cells self-renewal for prolonged time in culture (Rose-John, 2002) (Williams et al., 1988) . This ability is due to the binding of LIF with gp130 receptor that will activate the transcription of the Stat3 factor (Yoshida et al., 1994). This Stat3 activation represents a key transcriptional factor for ES cells self-renewal through activation of some target genes transcription after its translocation into the cells' nucleus (Niwa et al., 1998). So, using a culture medium supplemented with LIF and the 2i conditions, it is possible to maintain ES cells in culture, for prolonged time, retaining their self-renewing capacity and reducing significantly spontaneous differentiation events along time.

2.5.2 From Pluripotency to Cardiac Differentiation

The pluripotency properties in ES cells are maintained due to the expression and interactions between specific transcription factors. When we aim to characterize a ES cell line it is crucial to assess to the presence of some markers that will give us the true notion of the existence of pluripotency properties in the line. In this way, the *Oct4*, *Sox2*, *SSEA1* and *Nanog* are common used markers to characterize a mouse ES cell line and they are integrated in the panel of pluripotency markers of choice (Morey et al., 2015).

Oct4 belongs to the POU transcription factor family being highly expressed in the early embryos and germ cells, decreasing its protein expression during differentiation (Shi & Jin, 2010). The first data defining it as a regulatory candidate gene for pluripotent stem cell lineage show that, in *Oct4*-mutant mice, the blastocysts were well developed but the ICM was not composed by pluripotent cells, as opposed to what occurs in wild type mice (Nichols et al., 1998). Thus, the expression of *Oct4* is crucial to trigger the initial development of pluripotency properties in the ICM. Also, other study demonstrate that a critical amount of Oct4 is required in order to sustain the ES cells self-renewal, and up- or downregulation of this factor leads to primitive endoderm and mesoderm formation or loss of pluripotency consequently leading to dedifferentiation towards TE (Niwa et al., 2000). So, *Oct4* either can leads to pluripotency maintenance or to cell lineage specification.

Sox2 is defined as the transcription factor SRY-type high mobility group box 2, belonging to the SoxB1 subgroup which includes the *Sox1* and *Sox3* factors (Kamachi et al., 2000). Like in *Oct4* transcription factor, *Sox2* expression levels need to be kept within a certain range of values to maintain the self-renewal of ES cells. Using the downregulation and overexpression of this factor, it was showed that lower levels of Sox2 promote the differentiation of mouse ES cells into cells from the trophectoderm linage, and its overexpression could promote neuroectodermal differentiation (Zhao et al., 2004). Its expression is observed not only in the pluripotent lineage cells but also in multipotent cells derived from extraembryonic ectoderm (Avilion et al., 2003).

SSEA-1 (stage-specific embryonic antigen-1), also known as CD15, is classified as a cell surface antigen with a Lewis^x carbohydrate structure. Its expression is restricted to the early stage of mouse development starting at the 8-cell stage (Solter & Knowles, 1978). Also, it is a good cell surface marker to control ES cell differentiation because its expression is only verified in teratocarcinoma stem cells and ES cells and, consequently, absent in their differentiated cell lineages (Cui, 2004). *SSEA-1* is often used as a negative surface marker to test pluripotency in human stem cells (Martí et al., 2013).

Nanog consist in a homeodomain transcription factor critical for early embryo development according to its role in ICM cells' fate, as referred before, as well as regulating the maintenance of the pluripotent epiblast phase (Pan & Thomson, 2007). The level of Nanog proteins reaches the maximum peak at the morula stage until late blastocyst, and then become restricted to the epiblast and excluded from the primitive endoderm area. When implantation stage occurs, it is verified a downregulation in Nanog expression. However, it's still could be found in germ cells of E11.5 mouse embryos (Chambers et al., 2003). In vitro, Nanog is expressed in mouse and human ES cells and when low levels are detected, it is a signal that ES cells are starting to suffer differentiation (Pan & Thomson, 2007). Previous studies, proved that *Nanog* is one of the most important master regulators of the pluripotency state by discover its ability to maintain self-renewal of ES cells in absence of the LIF/gp130/Stat3 pathway in mouse cells (Chambers et al., 2003) (Mitsui et al., 2003). Also, Oct4 and Sox2 have been implicated in *Nanog* transcription process, during pluripotency maintenance, by the direct binding to its promoter verified both *in vivo* and *in vitro* (Rodda et al., 2005).

2.5.2.1 Cardiac Differentiation Program *in vitro*

Cardiac differentiation from mouse ES cells has become a routine and useful technique in many laboratories to study cardiovascular diseases and characterize diseases models. Since 1985, when was firstly prove that ES cells could spontaneous differentiate to cardiac functional cells *in vitro*, that culturing these cells as aggregates become an often used protocol (Doetschman et al., 1985). These ES cells' aggregates, called as Embryoid Bodies (EBs), consist in 3-dimensional structures capable to form the three germ layers (Doetschman et al., 1985). Using this capacity, EBs have been used to serve as models to recapitulate the early events of mammalian embryogenesis and study a range of differentiated cells derived from the germ layers (Desbaillets 2000) (Itskovitz-Eldor et al., 2000).

The differentiation protocol starts with the removal of LIF and other antidifferentiation factors from the culture medium. This step, allied to the hanging drop culture technique, will allow ES cells to encounter each other, as a stochastic event, forming the 3-dimentional EBs (Kurosawa, 2007). Usually, cells are cultured with a chosen precise density in hanging drops, in inverted bacterial-grade dishes, allowing the ES cells aggregation by gravity stimulus and by no adherence to the culture dishes (Figure 2.6) (Weitzer, 2006). However, this suspension culture technique has some inherent limitations and disadvantages, such as the heterogeneously in size and shape of the EBs that could led to lose of differentiation synchrony and a lower percentage of cardiomyocytes' production. Also, the culture conditions used for generation and maintenance of the ES cell lines (e.g. type of feeder cells, the medium, the source or batch of supplementation serum and even the characteristic handling of the scientist) could influence the EB development leading to unclear results (Weitzer, 2006). In this way, it is critical that the chosen culture protocol to form EBs led to a reproducible and homogeneous morphology. In order to get around this, in the last years, some investigators start to use a direct protocol to differentiate mouse and human cardiomyocytes in monolayer by adding a specific set of supplements (Activin A, BMP4, VEGF, and others) to the culture medium resulting in a high percentage of functional derived cardiomyocytes (Lian et al., 2013) (Kokkinopoulos et al., 2016). Nevertheless, this monolayer protocol approach could not be used to differentiate the *Cerl2*$^{-/-}$ ES cells, derived in this project, because the regular growth factors added possibly will masker the effect of the *Cerl2* KO gene by the direct cardiac pathways' stimulation. Also, the EB differentiation system seems to be the correct protocol in the present project, to mimic early cardiomyogenesis, according to the main role of the *Cerl2* during the embryonic developmental window in mouse.

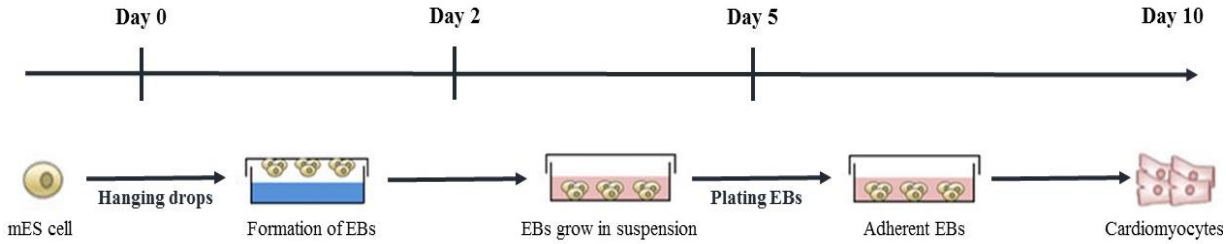

Figure 2.6: Schematic representation of the cardiomyocytes' differentiation using the hanging drop technique. The undifferentiated cells are maintained in culture for several passages with ES cell medium supplemented with LIF. Then, the desired cell suspensions are prepared in single drops, separated between each other's, and the plate lid is inverted. By gravity stimulus, ES cells start to aggregate in Embryoid Bodies (EBs), during 2 days, and then they continue to grow in suspension culture. At day 5, EBs are plated in gelatin-coated 6-well plates leading to cardiomyocytes differentiation and maturation until day 10 (figure modified from Bai et al., 2015).

After 24 hours, in hanging drops, ES cells are arranged in 3D aggregates resembling to the early morula structure in embryos, with irregular surfaces (Weitzer, 2006). During day 2, occurs a process of surface smoothness analogous to the morula compaction steps until blastocyst conformation. EBs continue to increase in size by the origin of primitive endodermal cells at its outer side, at day 3, through downregulation of the pluripotency genes and upregulation of *α-Fetoprotein (AFP)* gene (Weitzer, 2006). By days 4-5, its entire surface is covered with endoderm cells and the ES cells, situated in the inner side, start to differentiate to primitive ectoderm cells expressing positively *Vimentin* gene (Boheler et al., 2002). Meanwhile, mesoderm formation is induced confirmed by *Mesp-1* expression around day 4. This expression pattern occurs in the embryo at the E6.5 stage during PS establishment, marking the first cardiac progenitors that will populate the FHF and SHF (Saga et al., 1996). As a master regulator of cardiac cell-fate determination, previously studies clarified that overexpression of *Mesp-1*, in EBs culture, leads to an accelerated specific myocardial cell fate differentiation by regulating specific set of genes involved in cardiac specification (Lindsley et al., 2008) (Bondue et al., 2008). Then, after day 4, its expression in cardiac mesoderm specification become downregulated and specific early cardiac markers become upregulated. *Isl1* and *Nkx2.5* are the next transient genes to became highly expressed in EBs, giving the information of positive differentiation of cardiac progenitor cells. Comparing to the embryo model, *Nkx2.5* and *Isl1* are critical transcription markers against FHF and SHF cells' lineage, respectively (Kelly et al., 2014) (Cai et al., 2003). *In vitro*, within 4-6 days, progenitors expressing $Isl1^{+}$ and $Nkx2.5^{+}$ could originate cardiomyocytes, smooth muscle, pacemaker and endothelial cells being classified these as multipotent cardiovascular progenitors (Moretti et al., 2006).

At day 6, after plating, EBs are completely attached to the surface by the primarily proliferation of endoderm outer layer (Weitzer, 2006). Beating foci started to be visible in different areas, indicating the first signs of mature cardiac differentiation. These rhythmic areas are characterized by having a thick and elongated structure with arch-shaped ridges, phenotypically identical to those find *in vivo* myocardium (Doetschman et al., 1985). Until day 10, the spontaneously beating foci show identical action potentials' shape compared to those measured in primary cultures of embryonic cardiomyocytes and display the ability to develop adrenoreceptors (Wobus et al., 1991). Victor Maltsev and his colleagues, specifically isolated cardiomyocytes derived from EBs and, using the batch-clamp system, proved that these cells create different shapes of action potentials according to their spontaneous differentiation stage (Maltsev et al., 1993). This is explained by the maturation and increased number of ionic channels along the lineage specification. So, the most common genes used to specifically identify mature cardiomyocytes are *cTnT* and *α-MHC*, reaching its expression peak at day 10 of differentiation (Weitzer, 2006). It was proved that EBs transcribe *α-MHC* and tropomyosin isoforms (α-tropomyosin

and β-tropomyosin) in an appropriate developmental stage identical correlated to what occurs *in vivo* mouse embryos (Robbins et al., 1990) (Muthuchamy et al., 1993).

2.6 From *Cerberus-like 2* Gene to a Disease Model

Since the first ES cells derivation from early mouse embryos, as explained before, these cells have been reached an important role in understanding some human diseases. And more important, it was through them discover and correct derivation that Capecchi and Smithies, some years later, independently, discovered how homologous recombination between DNA segments can be used to modify regions of interest in mammalian genes (Thomas et al., 1986) (Smithies et al., 1985). Then, they used this knowledge to produce knockout (KO) mice. Since that time, the use of this mutant mice has become a useful tool in biomedical studies, being routinely used.

So, through a generation of mouse models containing specific null alleles, that were Mendelian-inheritable traits, it is possible to mimic, in mice, human diseases involved in deficient heart formation. Despite the differences in complexity between human heart and the mouse heart, both are composed by the same number of chambers: two ventricles and two atria. Still, the mouse is considered a useful model to study human diseases since 99% of its genes have equivalents in human genes with highly conserved biological pathways between them (Waterston et al., 2002).

According to these developments, KO mice started to be used in order to study the roles of *Cerl2* gene during heart formation in the early mouse development. These particularly mice were generated through the chimera technique using ES cells derived from 129-strain. Firstly, a cDNA clonal vector was isolated, by screening the 129/Ola genomic mouse library, containing only partial sequence information for the *Cerl2* gene (Marques et al., 2004). Using a cDNA clonal vector, its second exon fragment was replaced by insertion of a gene-selection marker in the targeting vector, leading to the inactivation of the *Cerl2* gene sequence (Marques et al., 2004). The most common one, the gene that confers resistance to neomycin toxic agent, was used in this step allied with the *lacZ* sequence. This *lacZ* cassette is derived from *Escherichia coli*, encoding enzyme β-galactosidase, and acts like a reporter gene helping to track the target gene's expression patterning in the mutant ES cells (Hall et al., 2009). Using the electroporation technique for the ES cells, the complex machinery of its nucleus start to activate homologous recombination that will replace the endogenous gene for the corresponding region of the insert target vector (Capecchi, 2005). Then, one KO ES cell clone was inserted by blastocyst cavity injection in a host mouse and implanted into the uterus of a female mouse. However, recently a new genetic reprogramming approach called CRISPR/Cas9 emerged in the scientific community. Quickly, this novel technique become the first choice tool for modeling disease in mouse according to the simplicity and less consuming time compared to the described chimera protocol (Cong et al., 2013) (Jinek et al., 2013) (Mali et al., 2013).

Previous studies showed that a significant number of *Cerl2*$^{-/-}$ mutants mice died within 48 hours after birth, displaying various laterality defects such as pulmonary isomerism, thoracic situs inversus and cardiovascular malformations, like ventricular septation and incomplete atrial (Marques et al., 2004). So, it was important to study the consequences involved beyond *Cerl2* loss of function, independently of the presence of laterality defects that could influence the cardiac structure and function in mice and confound the true implications of this gene. And, recently, *Cerl2*$^{-/-}$ mice without this type of malformations were investigated, showing left ventricular hypertrophy with enlarged myocardial walls comparing with the wild-type mice (Araújo et al., 2014). Cardiac function in *Cerl2*$^{-/-}$ neonates was evaluated, using echocardiography exams, showing a compromise in cardiac electrophysiology – decreased in heart rate and left ventricular mass index as well as reduced ascending aorta artery peak

velocity (Araújo et al., 2014). In this way, it is notorious the implication of the characteristic phenotype in *Cerl2*$^{-/-}$ neonates with impaired left ventricular systolic function. Surprisingly, this phenotype was associated to an increment in cardiomyocyte proliferation that was translated in an increased mitotic index (Araújo et al., 2014). Also, the results prove that the increment in cardiomyocyte mitotic events is translated in hyperplasia and did not occur as a response to a stimulus from cardiac cell's apoptosis discarding the myocardial hypertrophy through excessive deposition of extracellular matrix components. This was demonstrated by increased levels of *Ccnd1* relative expression, consisting in cyclin-D1 that normally regulates the decision of G1 mitosis progression (Araújo et al., 2014) (Quelle et al., 1993). Allied to these, the team detected an increase of Smad2 phosphorylated levels in hearts at neonatal and E13 stage. In the absence of Cerl2 antagonist for Nodal signaling, the molecular pathway continue its positive looping leading to more Smad2 proteins activation (Araújo et al., 2014).

To further clarify the role of *Cerl2* during embryogenesis, a generation of a corresponding KO ES cell line would be a useful *in vitro* model. Using these tool, cardiomyocytes could be differentiated providing valuable information to answer to the remain questions related to the possible role of this gene in cardiomyogenesis pathways.

3. Materials and Methods

3.1 Mice

The animals were maintained in an air-conditioned room at 21ºC, in a 12-hour light-dark cycle, and fed with autoclaved mouse food and tap water in microisolator cages for housing.

The mouse line used in this project was the *Cerl2* knockout (*Cerl2*$^{-/-}$) on background 129/Sv, previously generated by the team using the chimera technique explained in Chapter 2 (Marques et al., 2004). Two heterozygous *Cerl2*$^{-/-}$ females were mate with one heterozygous *Cerl2*$^{-/-}$ male, in each cage, at afternoon. Normally, copulation occurs around midnight (Suckow et al., 2001). In the following morning, vaginal plugs were checked to confirm successful mating. The plug consists in a whitish mass occluding the entrance of the mouse vagina. It's a consequence of the coagulation of some proteins present in the ejaculated semen from the male mouse (Suckow et al., 2001). These structures start to disappear for 8-24 hours after copulation, so the vaginal plug detection was always performed before noon. Embryonic stage E0.5 was considered at noon of the plugs detection day.

3.2 Derivation and culture of Mouse Embryonic Fibroblasts (MEFs)

Pregnant females at E13.5 were sacrificed by cervical dislocation and the uterine horns were surgically removed. The embryos were removed and placed into a Petri dish containing ice-cold PBS (Gibco® Life Technologies). Using forceps, amniotic sacs were cut in order to discard the head, internal and thoracic organs from the embryos.

The eviscerated embryos were washed again in 2 mL of PBS, in a clean 6-well culture plate, and were diced into small fragments. An incubation with 700 µL of trypsin 1x (Gibco® Life Technologies) was performed, for 5 minutes, to break cells' ligations and get cells into suspension, and 7 mL of DMEM medium (Dulbecco's Modified Eagle Medium, Gibco® Life Technologies), supplemented with 10% (v/v%) FBS (Sigma-Aldrich), 1x Penicillin/Streptomycin (Gibco® Life Technologies) and 2mM L-glutamine (Invitrogen Life Technologies), was added in each one. Resuspension, up and down, was performed to improve cells detachment and, then, cells were centrifuged at 1000 rpm for 5 minutes, at room temperature. Carefully, the supernatant was removed and the cells' pellet was resuspended in freshly DMEM medium. The remaining cells from each embryo were plated on an individual 10-cm culture dish and incubated in a humidified atmosphere at 37ºC and 5% CO_2. This was considered Passage 0 (P0). After 24 hours, the cells' medium was renewed.

When 70-80% of confluence was reached, MEFs were frozen at P1. Firstly, the cells were incubated, for 5 minutes, with 1 mL of trypsin 1x and were put in 1 mL vials (1.0×10^6 cells) using 1 mL of freezing medium composed by 45% FBS, 10% DMSO (D2650, Sigma-Aldrich) and 45% DMEM medium, per vial, and they were maintained at -80ºC, until used.

3.2.1 Mitotic Inactivation of MEFs

At least 2 days before using as feeder layers for the ES cells, MEFs were defrosted resuspending them in 7 mL of DMEM medium and centrifuged at 1000 rpm for 5 minutes to discard the remaining freezing medium. Then, the pellets were again resuspended in fresh DMEM medium and plated onto previously 0.1% gelatin-coated 6-well culture plate (Sigma). Cells were incubated at 37ºC and 5% CO_2 and medium was changed every day.

When the cells reached 70-80% confluence, the medium was replaced with supplemented DMEM medium containing 10 µg/mL of mitomycin C (Sigma) and incubated for 2-3 hours. After, the cells were washed three times with PBS, freshly DMEM medium was added and then the MEFs were incubated at 37ºC and 5% CO_2 until used as feeder cells for mouse ES cells. The medium was renewed daily.

3.3 Derivation and Primary Culture of Mouse *Cerl2*$^{-/-}$ ES Cell Lines

Three days after vaginal plug detection, pregnant females were sacrificed by cervical dislocation and the uterine horns were surgically removed and immediately placed on pre-heated M2 culture medium (EmbryoMax®, Millipore).

The uterine horns were separated and the ovaries were removed, cutting near to the oviduct, under a stereomicroscope (Zeiss Stemi DV4). Then, blastocysts were flushed, using a pipette with M2 medium, and collected onto a Petri dish (Figure 3.1). To remove remaining maternal tissues, the blastocysts were washed twice, using M2 drops. An incubation with Acidic Tyrode's solution (137 mM NaCl; 2.7 mM KCl; 1.6 mM $CaCl_2.2H_2O$; 0.5 mM $MgCl_2.6H_2O$; 5.6 mM glucose; 0.4% Polyvinylpyrrolidone (PVP), pH 2.5) was done, for 1-2 minutes, to remove the zona pellucida.

One blastocyst was plated per well, in a 6-well plate, on mitotically inactivated MEF feeders, containing ES cell medium composed by Knockout-DMEM medium (Gibco® Life Technologies) supplemented with 15% FBS (HyClone, Thermo Scientific), 1% MEM Non-Essential Amino Acids (Gibco® Life Technologies), 1% Penicillin/Streptomycin, 2 mM L-glutamine and 0.1 mM β-Mercaptoethanol (Gibco® Life Technologies). In order to maintain pluripotency conditions, 5 x 10^4 U mouse LIF (ESGRO® Millipore) was added as well as 1 µM PD0325901 (Calbiochem® Millipore) and 2 µM CHIRON99021 (Calbiochem® Millipore) inhibitors. Blastocysts were incubated at 37ºC, 5% CO_2 for 48 hours, avoiding any disturbance during this period in order to allow its attachment to the feeder layer.

On day 3, after flushing, half of the medium was replaced with fresh one. During days 3-7, the outgrowths were monitored daily under an inverted microscope (10x objective, Axiovert 40 CFL, Zeiss) until they adapt the right morphology for performing the first passage. Also, medium was renewed every day.

At day 7, medium was removed and the cells were rinsed once with PBS. And, 500 µL of enzyme TrypLE™ Select 1x (Gibco® Life Technologies) was added, incubating for 5 minutes at 37ºC to allow dissociation of cells. After, 5 mL of medium was added to inactivate the enzymatic process. The cells were transferred onto new inactivated feeder layers. The incipient ES cell line is at Passage 1 (P1), and medium was replaced every day. After 3-4 days, ES cell colonies started to be observable.

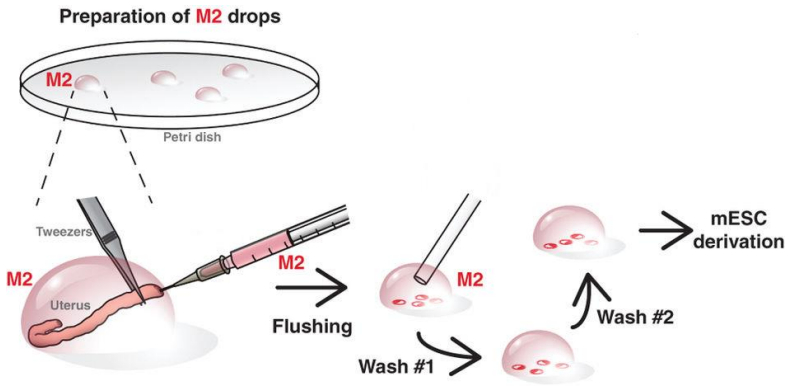

Figure 3.1: Overview of mouse blastocysts collection from female uterus. Embryos were flushed from the female uteri at E3.5 using M2 medium and washed in a series of M2 drops in order to remove maternal tissue debris (figure modified from Czechanski et al., 2014).

3.4 Subsequent Passaging and Culture of Mouse *Cerl2*$^{-/-}$ ES Cells

After P1, the *Cerl2*$^{-/-}$ ES cells were passed to 1:4 dilution factor in 6-well plates, when the right confluence was achieved, normally took two or three days after plating. At this stage, the cells were still cocultured with mitotically inactivated MEFs. Firstly, medium was removed and the cells were rinsed once with 2 mL of PBS and incubated with 500 µL of TrypLE™ Select 1x for 5 minutes at 37ºC. Then, cells were resuspended to disaggregate ES cells' colonies using 5 mL of ES cell medium. They were plated in fresh inactivated MEFs and incubated at 37ºC and 5% CO_2. In this stage, *Cerl2*$^{-/-}$ ES cells were at P2.

With the purpose to gradually adapt the cells to gelatin layers, MEFs feeder layers were discard after P3. Also, to have ample frozen stocks of ES cells, for the following experiments it was necessary to culture the cells in 100 mm dishes. In this way, firstly, culture plates were coated with 0.1% gelatin for 15-20 minutes at room temperature and, then, the excess was removed. To passage the cells, the medium was removed and they were rinsed once with 10 mL of PBS and then incubated with 1 mL of TrypLE™ Select 1x for 5 minutes at 37ºC. After this period, new ES cell medium was added, to stop the enzymatic reaction, and the volume of medium was adjusted according to the dilution factor intended.

3.5 Polymerase Chain Reaction (PCR)

For each *Cerl2*$^{-/-}$ ES cell line derived from mouse blastocysts, the mutant genotyping construction was confirmed by PCR technique comparing with the WT mouse's cells control. Then, the gender of the cells was identified also by PCR.

To do that, genomic DNA was extracted from each *Cerl2*$^{-/-}$ ES cell line. Firstly, cells were collected from culture, centrifuged at 1000 rpm for 5 minutes and re-suspended in 200 µL of Lysis Buffer GL and 25 µL of Proteinase K solution to promote lysis, included in Isolate II Genomic DNA kit (Bioline). The subsequent steps were done following the manufacturer's protocol.

The DNA samples were evaluated relating to quantity and quality using a spectrophotometer (Nanodrop 2000, Thermo Scientific). Only samples with 260/280 nm and 260/230 nm ratios equal or superior to 1.8 were considered. Posteriorly, all the PCR experiments were performed using a C1000 Touch™ Thermal Cycler (Bio-Rad).

3.5.1 Mutant Genotyping

In order to confirm the mutant genotyping in the mouse *Cerl2*$^{-/-}$ ES cell lines, a PCR was performed. The process consisted in an initial denaturation step at 95ºC for 4 minutes, followed by 30 cycles of denaturation at 95ºC for 1 minute, annealing step at 60ºC for 45 seconds and extension at 72ºC for 45 seconds. Also, the last extension step was done at 72ºC for 10 minutes. The reactions were prepared for a final volume of 25 µL, composed by 0.2 mM dNTPs, 1 µM of forward primer, 1 µM of primer lower 2, 1 µM of primer AA289c P3, 0.1 U/µL DreamTaq DNA polymerase, 2.5 µL of DreamTaq™ Buffer 10x and 50-70 ng of DNA sample. Details for each primer used for cells' genotyping are given in Table 3.1.

The PCR products were then separated on a 1% (w/v%) agarose (Grisp Research Solutions) gel dissolved in TAE 1x buffer. In order to intercalate between DNA chains, 5 µL of GreenSafe Premium (NZYTech) was added for a final volume of 100 mL of agarose gel. Agarose gel electrophoresis was performed in TAE 1x buffer, at a constant voltage of 80 V, running in parallel with the samples a 1Kb Plus DNA ladder. Then, the separated PCR products were visualized using Chemidoc (Bio-Rad) by UV-light exposure.

Table 3.1: Primers nucleotide sequences for PCR to determine the cells' genotyping.

Gene	Primers
Cerl2	GenCer2-fwd: 5' GGA AGA TTT TAT GCA AGC AAG AGT GTG G 3'
	Lower2: 5' GGT GAC TTC TTT TTT GCT TTA GCA GG 3'
	AA289c P3: 5' CAC ACA GCT GTT GCA GAA GAC 3'

3.5.2 Gender Determination

PCR was performed to amplify a specific region of *Sry* gene located on the Y-chromosome. The amplification process was performed through an initial denaturation step at 95ºC for 3 minutes to break hydrogen bonds, followed by 30 cycles of denaturation at 95ºC for 30 seconds, annealing of primers at 54.7ºC for 45 seconds and extension at 72ºC for 30 seconds. Then, a last extension step was done at 72ºC for 5 minutes allowing the complete amplification of the new strands which may have been incomplete. The reactions were prepared for a final volume of 25 µL, composed by 0.2 mM dNTPs, 1 µM of forward primer, 1 µM of reverse primer, 0.1 U/µL of DreamTaq DNA polymerase, 2.5 µL of DreamTaq™ Buffer 10x and 50-70 ng of DNA sample. Details for each primer used for gender determination are given in Table 3.2.

The PCR products were then separated on a 1% (w/v%) agarose (Grisp Research Solutions) gel dissolved in TAE 1x buffer. In order to intercalate between DNA chains, 5 µL of GreenSafe Premium (NZYTech) was added for a final volume of 100 mL of agarose gel. Agarose gel electrophoresis was performed in TAE 1x buffer, at a constant voltage of 80 V, running in parallel with the samples a 1Kb Plus DNA ladder. Then, the separated PCR products were visualized using Chemidoc (Bio-Rad) by UV-light exposure.

Table 3.2: Primers nucleotide sequences for PCR to determine the cells' gender.

Gene	Primers
Sry	Fwd: 5' AT GGA GGG CCA TGT CAA 3'
	Rev: 5' AC ACT TTA GCC CTC CGA 3'

3.6 Karyotyping

Firstly, the mouse *Cerl2*$^{-/-}$ ES cell lines were cultured until reached 50-70% confluency in the same conditions as described before. They were incubated with 20 ng/mL of colcemid (Invitrogen) in ES cell medium for 5 hours at 37ºC, to arrest cells in metaphase. Then, they were washed in PBS and incubated with 1 mL TrypLE™ Select 1x for 5 minutes at 37ºC. The detached cells were resuspended in 9 mL ES cell medium and centrifuged for 5 minutes at 1000 rpm. Supernatant was discard and the pellet was resuspended in 500 µL ES cell medium. After, 5 mL of preheated KCl 0.075 M were added in a drop-by-drop manner, to prevent cells' lysis, and the tube was carefully inverted to mix the solution. The mixture was incubated at 37ºC for 20 minutes. Three drops of fixation solution 3:1 methanol: glacial acetic acid were slowly added and cells were homogenized by tube inversion. Cells were again centrifuged for 5 minutes at 1000 rpm, the supernatant was discarded and the pellet slowly resuspended in 7 mL of fixative solution, drop-by-drop. Then, they were centrifuged for 5 minutes at 1000 rpm. The cells were re-fixed and re-centrifuged twice as described above before final re-suspension of the pellet in 2 mL of fixative solution. Samples were store at -20ºC until the subsequent steps were performed.

The G-banding technique and karyotype analysis were performed by cytogenetic technologists at the Department of Genetics, Faculty of Medicine of the University of Porto - São João Hospital. In total, 15 metaphases were evaluated for each ES cell line. And, only one final image was generated for each line.

3.7 Immunostaining for Markers of Pluripotency

The mouse *Cerl2*$^{-/-}$ ES cells from the derived lines were cultured in 24-well glass bottom plates, coated with 0.1% gelatin. Then, the cells were incubated until reached 50% confluency at 37ºC and 5% CO_2.

The cells were rinsed with 1 mL room-temperature PBS 1x and fixated with 4% PFA in PBS 1x for 15 minutes, at room temperature. Three washes with PBS 1x for 5 minutes each were performed to remove PFA remains. After, cells were incubated with PBS containing 0.1% Triton-X 100 (Sigma) for 30 minutes at room temperature. This incubation step is important when we want to access to intracellular and/or intraorganellar antigens, like NANOG and OCT4. The Triton-X 100 acts as detergent disrupting the hydrogen bonding in the phospholipid bilayer, improving the penetration of the antibodies (Fallis, 2010) . However, cells that would be incubated with the primary antibody against the membranal marker SSEA-1 were not permeabilized with Triton X-100 because that step would remove lipids from the cell's membrane causing its disruption of structure and, consequently, the loss of its specific antigens. Then, to block nonspecific antibody-binding sites, cells were incubated with Blocking Solution (1x PBS, 1% BSA, 0.05% sodium azide) for 30 minutes at room temperature.

Then, cells were incubated with the primary antibodies anti-OCT4, anti-NANOG and anti-SSEA1 overnight at 4ºC. After, four washes with Blocking Solution were performed for 10 minutes each and, then, cells were incubated with secondary antibodies at 4ºC overnight. Next day, cells were washed four times with Blocking Solution for 10 minutes, and incubated with DAPI for 40 minutes. The dilutions used for each antibody are listed in Table 3.3.

The cells were visualized and imaged with a Zeiss LSM 710 confocal microscope using a 40x water immersion objective. Images were taken in sequential mode and posteriorly adjusted in ImageJ program.

Table 3.3: Primary and secondary antibodies used for staining markers of pluripotency.

Antibody	Dilution	Source
Nanog anti-rabbit	1:150	Abcam
Oct4 anti-rabbit	1:150	Abcam
SSEA-1 anti-mouse	1:50	Abcam
DAPI	1:1000	Panreac AppliChem
Alexa Fluor® 594 Donkey anti-mouse IgG	1:300	Jackson ImmunoResearch Laboratories
Alexa Fluor® 594 Donkey anti-rabbit IgG	1:300	Jackson ImmunoResearch Laboratories

3.8 Embryoid Bodies Formation

The undifferentiated *Cerl2*$^{-/-}$ ES cells in culture were used to test the pluripotency potential and spontaneous differentiation by the hanging droplet method. Firstly, cells were washed with 10 ml of PBS 1x and then incubated with 1 mL of TrypLE^{TM} Select 1x for 5 minutes at 37ºC. After, 9 ml of ES cell medium was added and cells were dissociated into a single cell suspension. Cells were centrifuged for 5 minutes at 1000 rpm and resuspended in fresh ES cell medium without LIF and the 2i. Also, cells were counted using a Neubauer chamber and a cell suspension solution was prepared with a final concentration of $2.5x10^4$ cells/mL. Cells were plated as 20 µL drops (500 cells), using a multichannel pipette, on the base of an anti-adherent Petri dish and it was inverted into the lid to allow growing of EBs in drop suspension (day 0). Also, 8 mL of PBS 1x was added to the lid to provide a humidified environment. The cells were incubated at 37ºC and 5% CO_2 for 48 hours (days 1 and 2). Then, Petri dishes were inverted to the original position and 10 mL of fresh ES cell medium without LIF and 2i was added. EBs were cultured in suspension until day 5 changing half of the medium and, then, they were plated onto 0.1% gelatin coated wells and incubated until day 10 to promote spontaneous differentiation. The culture medium was renewed every day.

3.9 Immunostaining for Markers of Germ Layers' Differentiation

The mouse *Cerl2*$^{-/-}$ ES cells from the derived lines were cultured in hanging drops on the base of an anti-adherent Petri dish and, the, inverted into the lid. The cell suspension solution was prepared as described in the previous topic.

At the day 10 of differentiation, EBs were rinsed with 1 mL room-temperature PBS 1x and fixated with 4% PFA in PBS 1x for 30 minutes, at room temperature. Three washes with PBS 1x for 5 minutes each were performed to remove PFA remains. After, cells were incubated with PBS containing 0.1% Triton-X 100 (Sigma) for 1 hour at room temperature. Then, to block nonspecific antibody-binding sites, cells were incubated with Blocking Solution for 30 minutes at room temperature.

Then, cells were incubated with the primary antibodies anti-AFP, anti-α-ACTININ and anti-VIMENTIN overnight at 4ºC. After, six washes with Blocking Solution was done for 10 minutes each, and cells were incubated in secondary antibodies at 4ºC overnight. Next day, cells were washed six times with Blocking Solution for 10 minutes, and incubated with DAPI for 40 minutes. The dilutions used for each antibody are listed in Table 3.4.

The cells were visualized and imaged with a Zeiss LSM 710 confocal microscope using a 40x water immersion objective. Images were taken in sequential mode and posteriorly adjusted in ImageJ program.

Table 3.4: Primary and secondary antibodies used for staining markers of germ layers' differentiation.

Antibody	Dilution	Source
AFP anti-goat	1:100	Santa Cruz Biotechnology, Inc.
α-Actinin (Sarcomeric) anti-mouse	1:100	Sigma-Aldrich™
Vimentin anti-rabbit	1:50	Sigma-Aldrich™
DAPI	1:1000	Panreac AppliChem
Alexa Fluor® 594 Donkey anti-mouse IgG	1:300	Jackson ImmunoResearch Laboratories
Alexa Fluor® 594 Donkey anti-rabbit IgG	1:300	Jackson ImmunoResearch Laboratories
Alexa Fluor® 488 anti-goat IgG	1:1000	Thermo Fisher Scientific

3.10 Cardiac Differentiation of ES cells

E14 ES cells and *Cerl2*$^{-/-}$ ES cells were cultured through several passages with decreasing doses of 2i, dividing the dose volume of these inhibitors by two at each passage. Then, the ES cells were cultured and maintained using only the LIF supplementation without 2i.
Then, to initiate the cardiomyocytes' differentiation the EBs protocol was used, as described before. Firstly, the ES cells were cultured in hanging drops for 48 hours (days 1 and 2 of differentiation) until formed the EBs aggregations. From day 2 to day 5, EBs derived from the KO line and the control line (E14) were cultured in suspension and its growth was daily monitored with an inverted microscope (10x objective, Axiovert 40 CFL, Zeiss). Then, EBs were plated onto each 0.1% gelatin coated 6-wells and incubated until day 10 of differentiation. During this period, the morphology of proliferative outgrowths was regularly observed and beating foci areas were counted under the inverted microscope at different time points of differentiation.

3.11 RNA Extraction and cDNA Synthesis

RNA was extracted from mouse *Cerl2*$^{-/-}$ ES cells, MEF cells and EBs, at several days of differentiation, using 350 µL TRI Reagent® (Sigma-Aldrich) to promote lysis. An equal volume of 100% ethanol was added and samples were centrifuged at 12000 xg for 30 seconds, to precipitate the DNA and RNA. After, the samples were treated using the Direct-zol™ RNA MiniPrep Kit (Zymo Research) by following the manufacturer's protocol and using the solutions provided in the kit. The purified RNA samples were eluted in 40 µL of RNase free water, available in the indicated Kit.

The RNA samples were evaluated relating to quantity and quality using a spectrophotometer (Nanodrop 2000, Thermo Scientific). Only samples with 260/280 nm and 260/230 nm ratios equal or superior to 2.0 were considered. Then, the isolated total RNA for all samples were immediately stored at -80ºC for future experiments.

First strands cDNA were synthesized through reverse transcription reaction, which is composed by two steps. Firstly, each reaction composed by 1 µg of RNA, 0.5 µg of Oligo (dT) primers and RNase-free water up to 11.5 µL were incubated at 65ºC for 5 minutes. This step consists in the annealing of the

Oligo (dT) primers with the single strand of RNA template. Then, a master mix solution was added to the previous reaction, containing 4 µL of 5x Reaction Buffer, 40 U/µL of RiboLock RNase Inhibitor, 200 U/µL of RevertAid Reverse Transcriptase and 10 mM of dNTP, making a total 20 µL volume per each. In this stage, the PCR tubes were incubated at 42ºC for 1 hour followed by the step of Reverse Transcriptase enzyme denaturation at 70ºC for 10 minutes. At this stage, DNA strands were polymerized followed by the deactivation of the reverse transcriptase enzyme. Finally, cDNA samples were 1:10 diluted with RNase-free water and stored at -21ºC until used.

3.12 qRT-PCR

Triplicate reactions were performed in 96-well plates using optical sealing tape for a 15µL total volume for each. Each qRT-PCR reaction contained 7.5 µL of power SYBR® Green Master Mix (Applied Biosystems), 2 µL of cDNA, 0.1 µM of each forward and reverse primers and ultrapure water up to the final desired volume. The oligonucleotide primer sequences used and their annealing temperatures are listed in Table 3.4. The amplification and fluorescent detection was performed with Applied Biosystems 7300 Real-Time PCR machine. The conditions of amplification of target sequences were as follow: initial step of denaturation at 95ºC for 10 minutes, followed by 40 cycles of denaturation step at 95ºC for 30 seconds, annealing for 15 seconds at the gene-specific annealing temperature (Table 3.5) and an extension step at 72ºC for 30 seconds. Relative quantification of expression was performed using the ddCt method (Bustin, 2000) and normalized to GAPDH as housekeeping gene and with E14 ES cell line as reference.

Table 3.5: qRT-PCR primers used.

Gene	Primers	Annealing Temperature (ºC)
Nanog	Fwd 5’ AGG GTC TGC TAC TGA GAT GCT CTG 3’ Rv 5’ CAA CCA CTG GTT TTT CTG CCA CCG 3’	61
Oct4	Fwd 5’ AGT ATG AGG CTA CAG GGA CA 3’ Rv 5’ CAA AGC TCC AGG TTC TCT TG 3’	61
Sox2	Fwd 5’ CGA GAT AAA CAT GGC AAT CAA ATG 3’ Rv 5’ AAC GTT TGC CTT AAA CAA GAC CAC 3’	56
Mesp-1	Fwd 5’ TGT ACG CAG AAA CAG CAT CC 3’ Rv 5’ TTG TCC CCT CCA CTC TTC AG 3’	61
Isl1	Fwd 5’ CCT GTG TGT TGG TTG CGG CA 3’ Rv 5’ GGG CAC GCA TCA CGA AGT CG 3’	61
Cerl2	Fwd 5’ GCA GAG AGT AGC TGC TGG TGT GCC TTT 3’ Rv 5’ CGG CAC ACA GCT GTT GCA GAA GAC TAC 3’	68.3
Ccnd1	Fwd 5’ CAA ATG GAA CTG CTT CTG GTG AAC AA 3’ Rv 5’ GGA GGG TGG GTT GGA AAT GAA CTT 3’	63
cTnT	Fwd 5’ GGA AAT CCA AGA TCA CTG CCT CC 3’ Rv 5’ GGG CAC TGA GGG ACA GAC CA 3’	60
Nkx2.5	Fwd 5’ CCA CTC TCT GCT ACC CAC CT 3’ Rv 5’ CCA GGT TCA GGA TGT CTT TGA 3’	60

α-Mhc	Fwd 5’ GAT GGC ACA GAA GAT GCT GA 3’ Rv 5’ CTG CCC CTT GGT GAC ATA CT 3’	60
Gapdh	Fwd 5’ AAG AAG GTG GTG AAG CAG GC 3’ Rv 5’ GCC TCT CTT GCT CAG TGT CC 3’	61

3.13 Statistical Analysis

Statistical Analysis was performed using *GraphPad Prism 6* software for Windows (GraphPad Software, Inc; San Diego California, USA). All the experimental values are reported as mean ± SD.

In case of the RT-PCR experiments, statistical differences between the two groups (mutant and control groups) were determined applying the unpaired Student’s t-test. Also, one-way ANOVA test was applied when more than two groups were compared. To reject the null hypothesis, the probability values of *P<0.05 were considered statistically significant.

4. Results and Discussion

4.1 Generation of Mouse *Cerl2*$^{-/-}$ ES Cell Lines

According to the reported functions of Cerl2 proteins for a correct establishment of the L-R axis during cardiogenesis, also it was hypothesized that these molecules could be involved in the main processes of cardiomyogenesis. With the purpose to uncover the role of Cerl2 in the mechanisms of cardiac mesoderm differentiation, ES cells were used as the preferred disease model. Taking advantage of their capacity to differentiate into all cell lineages, it is possible to mimic *in vitro* the biological mechanisms that lead to the abnormal phenotype previously reported in the mutant mice (Nishikawa et al., 2007). So, to study the possible roles of *Cerl2* on the number of *in vitro* produced cardiomyocytes, three independent mouse ES cell lines were successfully derived from knockout (KO) mouse blastocysts. To improve chances of positive copulation, two females were mated with one male, at afternoon, in each cage. In the morning after, plugs were checked and detected by the presence of a whitish mass occluding the entrance of the mouse vagina. Then, it was considered that successful copulation occurred and pregnant females were separated into new cages defining stage E0.5. To take access to the blastocysts, pregnant females were sacrificed three days after plugs detection, i.e. at stage E3.5. Performing a flushing technique was possible to remove the blastocysts from inside the female uterus, using M2 medium that allows the collection and handling of embryos for a prolonged time, at room temperature, without the risk of damaged their biological properties. Then, the blastocysts were incubated with Acidic Tyrode's solution to disrupt the zona pellucida (Khalifa et al., 1992). After several trials, this demonstrated to be a crucial step to promote blastocyst hatching, because without using this solution it was observed that blastocysts continued to grow in suspension culture and eventually lost the desired properties. The mouse blastocysts were plated in mitotically MEFs and incubated until completely attached to the feeder layers, with ES cell medium supplemented with LIF and the 2i to improve the efficiency of retaining their pluripotency properties (Figure 4.1). Despite the amount of LIF naturally secreted by the MEF cells, it was necessary to perform the medium supplementation with chemical LIF (Ma et al., 2012). This was a necessary step to achieve the minimum concentration value required for maintenance of self-renew and pluripotency state because feeder layers secret factors in variable amounts during culturing. The optimal concentration value used was corresponding to the commercial product datasheet.

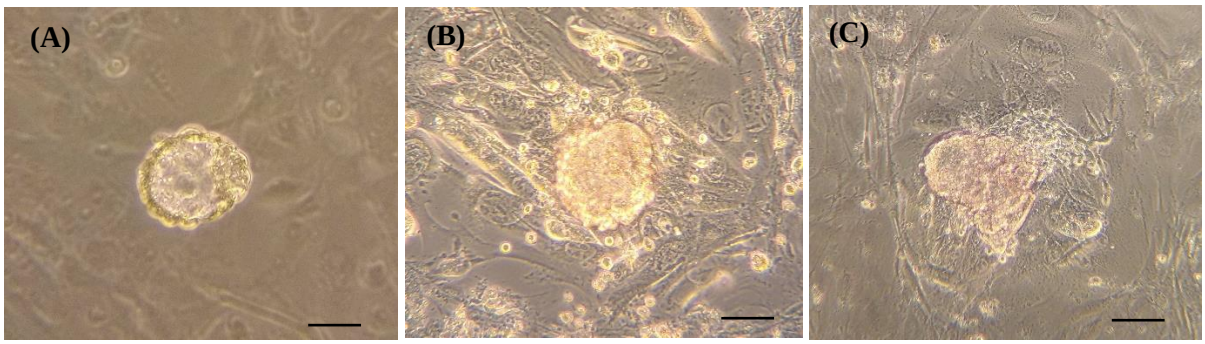

Figure 4.1: First steps of ES cells derivation from *Cerl2* KO mouse blastocysts. (A) Morphology of mouse blastocyst at stage E3.5, with well-defined ICM and blastocyst cavity; (B) Morphology of blastocyst hatched on MEF feeder at day 3 after collection; (C) At day 7, outgrowths were completely formed. Scale bars: 100 μm.

Until day 7, blastocysts expanded in culture and clusters of outgrowths started to be visible. Then, it was time to trypsinized the aggregation of pluripotent cells allowing the expansion of the first *Cerl2*$^{-/-}$ ES cells that will aggregate in colonies. As it is well documented, ES cells grow as packed colonies and show specific morphologic characteristics when they are visualized in an inverted microscope (Czechanski et al., 2014). Cells morphology was daily accessed during culture using an inverted microscope: *Cerl2*$^{-/-}$ ES cell colonies, from the three different lines, show oval morphology with clear light boundaries with a large nucleus compared with a reduced cytoplasm (Figure 4.2). Also, it was notable that some cells started to spontaneous differentiate in an insignificant frequency being this a positive factor of the action of the 2 inhibitors used in the culture medium system. Through the use of the chemical CHIR99021 inhibitor, the activity of GSK3 is blocked and self-renewal in ES cells is maintained, while the addition of the chemical PD0325901 inhibitor reduces cells differentiation by targeting MEK proteins and blocking the activation of Erk signaling cascade (Ying et al., 2008).

The *Cerl2*$^{-/-}$ ES cells were cocultured with freshly MEFs feeders up to Passage 3 to promote an efficient derivation with a lower spontaneous differentiation rate due to the sustentation and release of cytokines that inhibit ES cells' differentiation (Llames et al., 2015). For subsequent passages, the cells were cultured on 0.1% gelatin-coated plates to gradually adapt to this layer type allowing the decrease of contaminations risk and consuming time and money compared to the feeder layers. But the main reason for this change was to discard false results during the future experiments of differentiation. It is known the target function of some of the soluble factors released by the MEFs, but others are still unknown (Tamm et al., 2013). In this way, the continued use of these cells as feeder layers could possibly mask some normal process occurring during cardiomyogenesis or even cause inhibition/stimulation of some undesirable signaling pathways.

During these experiments, about 19 blastocysts were collected in total from pregnant females. However, just 8 blastocysts were at the pretended morphology stage and correctly attached to the inactivated MEF feeder layers forming outgrowths. During the entire protocol, only 3 of them could successfully originate *Cerl2*$^{-/-}$ ES cells. Taking this account, this *in vitro* derivation technique showed a lower efficiency (approximately 16%) in establishing ES cells from *in vivo* developed blastocysts.

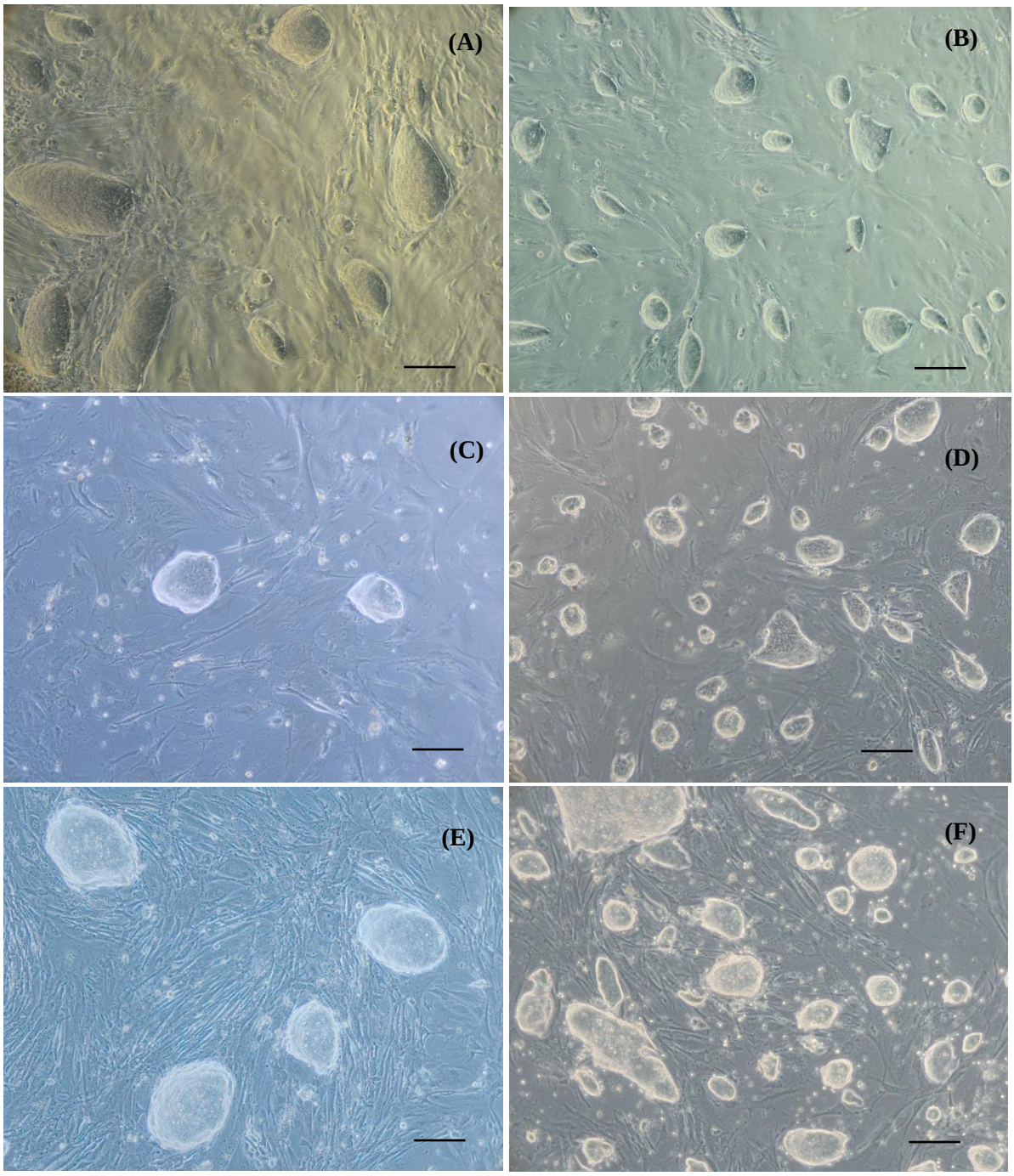

Figure 4.2: Morphology of *Cerl2*$^{-/-}$ ES cell colonies cocultured with MEFs at Passage 1 and Passage 2 from the derived lines. (A) ES cells from Embryo 1 at P1; (B) ES cells from Embryo 1 at P2; (C) ES cells from Embryo 5 at P1; (D) ES cells from Embryo 5 at P2; (E) ES cells from Embryo 6 at P1; (F) ES cells from Embryo 6 at P2. In the present images, the colonies show an oval morphology with lightly boundaries characteristic of ES cells. Spontaneous differentiation is not significantly notorious. Scale bars: 100 µm.

4.2 Characterization of the Derived Mouse *Cerl2*$^{-/-}$ ES Cell Lines

To use a derived KO ES cell line for future experiments it is crucial to characterize it relating to its chromosomic and genetic stability, pluripotency and differentiation capacities (Czechanski et al., 2014). To define *Cerl2*$^{-/-}$ ES cells populations demonstrating their pluripotency, standard protocols were performed on the three successfully derived lines.

Firstly, to confirm the KO genotype of the *Cerl2*$^{-/-}$ ES cells, the PCR technique was performed. Using specific pairs of forward and reverse primers, it was amplified the KO allele of the *Cerl2* gene from genomic DNA of KO and wild type (WT) cells, this last used as a negative control (Figure 4.3). The primer GenCer2-fwd was previously designed as a common forward primer annealing with both WT and KO alleles (Marques et al., 2004). Its starting annealing point is located upstream of the lacZ cassette insertion point. The reverse primer Lower2 was designed to anneal with the *Cerl2* WT allele, starting the annealing process in the 3' region of the corresponding end insertion point of the neomycin replacement cassette in the KO allele (Marques et al., 2004). As a reverse primer, specifically against the KO allele, the AA289c-P3 primer was used. This annealed in the 5' region within the lacZ cassette (Marques et al., 2004). In this experiment, a genomic DNA template from an adult *Cerl2* KO mouse was used as a positive control and a genomic DNA template from an adult WT mouse was used as a negative control. Also, a control without DNA was applied to discard false amplifications in PCR reactions. The results confirm the expected mutant genotyping for the three ES cell lines by the resulting product band of 500 bp, similar to the band obtained for the positive KO control. In case of the WT mouse, the resulting band size is 300 bp. Although the same amount of genomic DNA (70 ng) used in all samples, a product band with lower intensity in the *Cerl2*$^{-/-}$ ES cells derived from the Embryo 1 is evident. It could be caused by temporal degradation of the DNA sample or initial contamination that was not determined by the spectrophotometer reading.

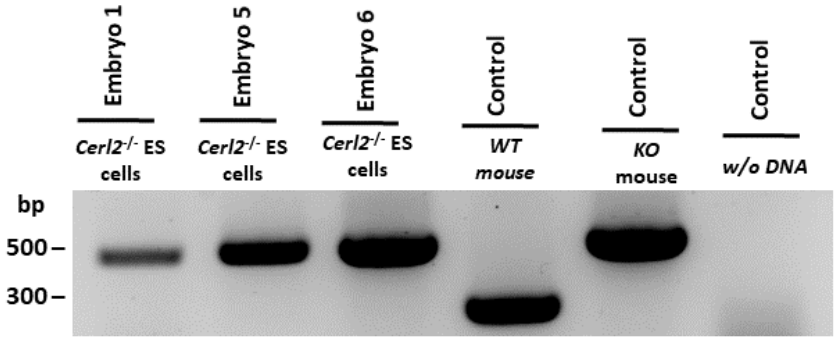

Figure 4.3: Mutant genotyping of the derived *Cerl2*$^{-/-}$ ES cells confirmed by PCR. Product bands with 500 bp size were detected in the three lines of *Cerl2*$^{-/-}$ ES cells derived and, also, in the adult KO mouse used as positive control. In opposition, the PCR product for the sample of the WT mouse resulted in a 300 bp band.

Then, a quickly and simply gender identification was also done by a PCR experiment. The male gender identification resulted by the positive amplification of a specific region of the *Sry* gene classified as the master regulator involved in early male phenotype (Polanco & Koopman, 2007). The product size is 247 bp and the results were visible through an existence of a band of this size, when ran in 1% agarose gel. With this technique, it was possible to simply identify that two *Cerl2*$^{-/-}$ ES cell lines are male (derived from Embryos 1 and 5) and the other one is female (derived from Embryo 6) (Figure 4.4). As positive and negative controls, genomic DNA samples from two adult male mice and two adult female mice were used. Again, to discard false amplifications, a PCR reaction control without DNA was used.

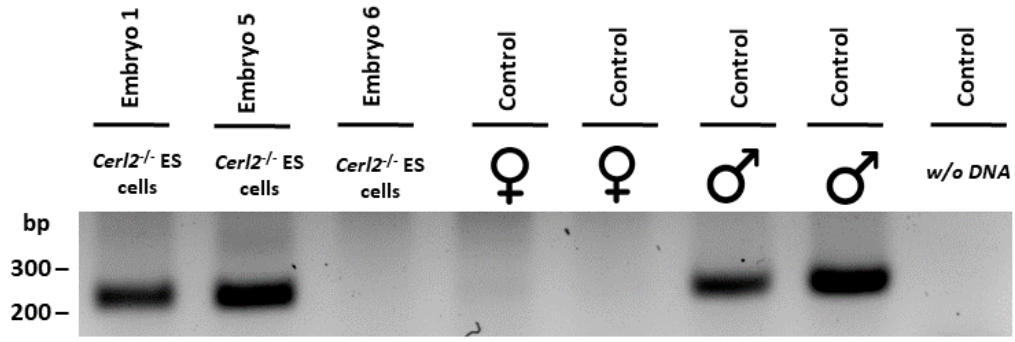

Figure 4.4: *Sry* gene expression revealed by PCR. A product band with 247 bp size was detected in male *Cerl2*$^{-/-}$ ES cells derived from Embryos 1 and 5 and, also, in both male mouse controls. So, it is shown that the absence of a band in DNA sample from Embryo 6 revealed a female gender in concordance with the two negative controls (from adult female mice).

4.2.1 Karyotype

In order to check the chromosomic integrity and stability, karyotyping was performed. Firstly, the ES cells were arrested in the metaphase stage during cell mitosis division at Passage 7. By using Colcemid solution, their growth cycle was affected in especially at microtubules' level. This mechanism of action is based on the ability to bind to tubulin dimers inhibiting its polymerization (Jordan & Wilson, 2004). Since tubulin heterodimers form microtubules, they will not be capable to sustain chromosomic segregation and, consequently, mitotic divisions will stop at metaphasis stage. So, using the G-banding staining technique, the derived *Cerl2*$^{-/-}$ ES cells were analyzed and 15 metaphases were evaluated, in total, for each line. Each chromosome shows a specific pattern of alternately light and dark regions, representing the negative G bands and the positive G bands, respectively. The regions marked with G bands are composed of AT-rich DNA and gene-poor, while the light regions have more GC-rich DNA characteristic of active genes with transcriptional activity (Bickmore, 2001). Then, during karyotyping analysis, each chromosome could be paired with its homologous by looking for the similarities in the approximately same length, centromere position and staining pattern.

The results show a normal chromosomic number for the three lines and there were not detected any translocation. Likewise, the karyotype results confirmed the gender of each line firstly obtained by the PCR technique. Thus, all the *Cerl2*$^{-/-}$ ES cell lines are euploid, composed by 40 chromosomes, being the cells derived from Embryo 1 and Embryo 5 male gender (40, XY) and the cells derived from Embryo 6 female gender (40, XX) (Figure 4.5).

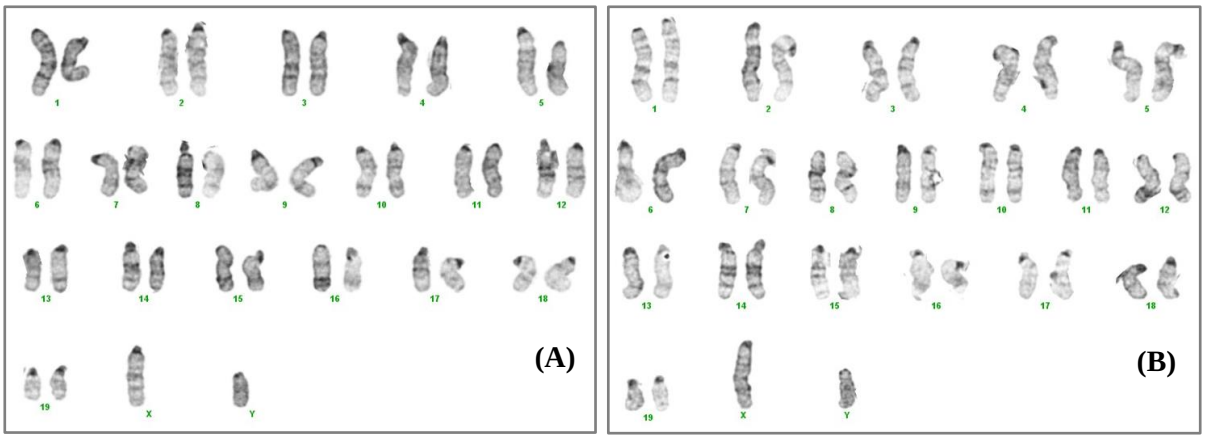

Figure 4.5: Karyograms of the derived *Cerl2*$^{-/-}$ ES cell lines, obtained by G-banding staining at Passage 7: (A) from Embryo 1; (B) from Embryo 5; and (C) from Embryo 6.

4.2.2 Pluripotency Properties

To validate pluripotency properties of the derived cells, firstly protein expression was confirmed using the immunofluorescence technique at Passage 5. At this stage, some inactivated MEFs were still present in the mouse *Cerl2*$^{-/-}$ ES cell cultures, and they were used as a negative control, in this experiment, because this type of cells does not express pluripotency markers. All ES cell colonies derived from Embryo 1, Embryo 5 and Embryo 6 expressed stem cell positive nucleus markers – NANOG and OCT4 – and the surface marker SSEA-1 (Figure 4.6 and Appendix A1). These markers were similarly expressed between the three lines, without a notorious difference in pluripotency properties. As a control of cellular quantification, cells were stained with DAPI that exclusively marks DNA in the nucleus, more specifically the A-T rich regions.

Comparing the merged staining images, it is noticed that some cells present outside of the colonies' region do not show positive signal for the NANOG and OCT4 markers, being these nuclei of the mouse fibroblasts. In the other side, in the case of a sporadic number of cells, localized at the colonies' borders, that do not express NANOG and OCT4 markers it is an indication of spontaneous differentiation and start losing of pluripotency expression.

Then, the expression of pluripotency genes was tested by quantitative RT-PCR at Passage 6. Using this technique, relative gene level for *Nanog*, *Oct4* and *Sox2* was evaluated for the *Cerl2*$^{-/-}$ ES cells for each derived line. All gene expression levels are relative to RNA extracted from a stabilized ES cell line, commercially named E14, and currently used in our Lab as a control line. It was selected for these experiments and posterior ones as a control line according to its 129/Sv background, the same as the *Cerl2*$^{-/-}$ ES cells, and its *wild-type* genotype. Also, RNA extracted from MEFs was used as a negative control. All values were normalized using *GAPDH* gene as an endogenous control, because its expression level does not diverge significantly between samples extracted from different types of cells. *GAPDH* is considered a housekeeping gene, since it is involved in mechanisms that maintain basal cellular functions such as glycosylation, so is expected that cells express it at a constant level (Eisenberg & Levanon, 2013). The values of the relative mRNA expression, for each cell line, was calculated considering the mean of Ct levels referred for each gene and normalized to the corresponding mean of Ct levels for the *GAPDH* gene. The Ct values correspond to the cycle where the amplification curves intersect the threshold line (Nolan et al., 2006). So, lower Ct values indicate a rapid amplification reaction by the presence of high amounts of the target cDNA sample while higher Ct levels show time-delayed cDNA amplification reactions, resulted by the lower or inexistent amount of the desired nucleotide template (Nolan et al., 2006).

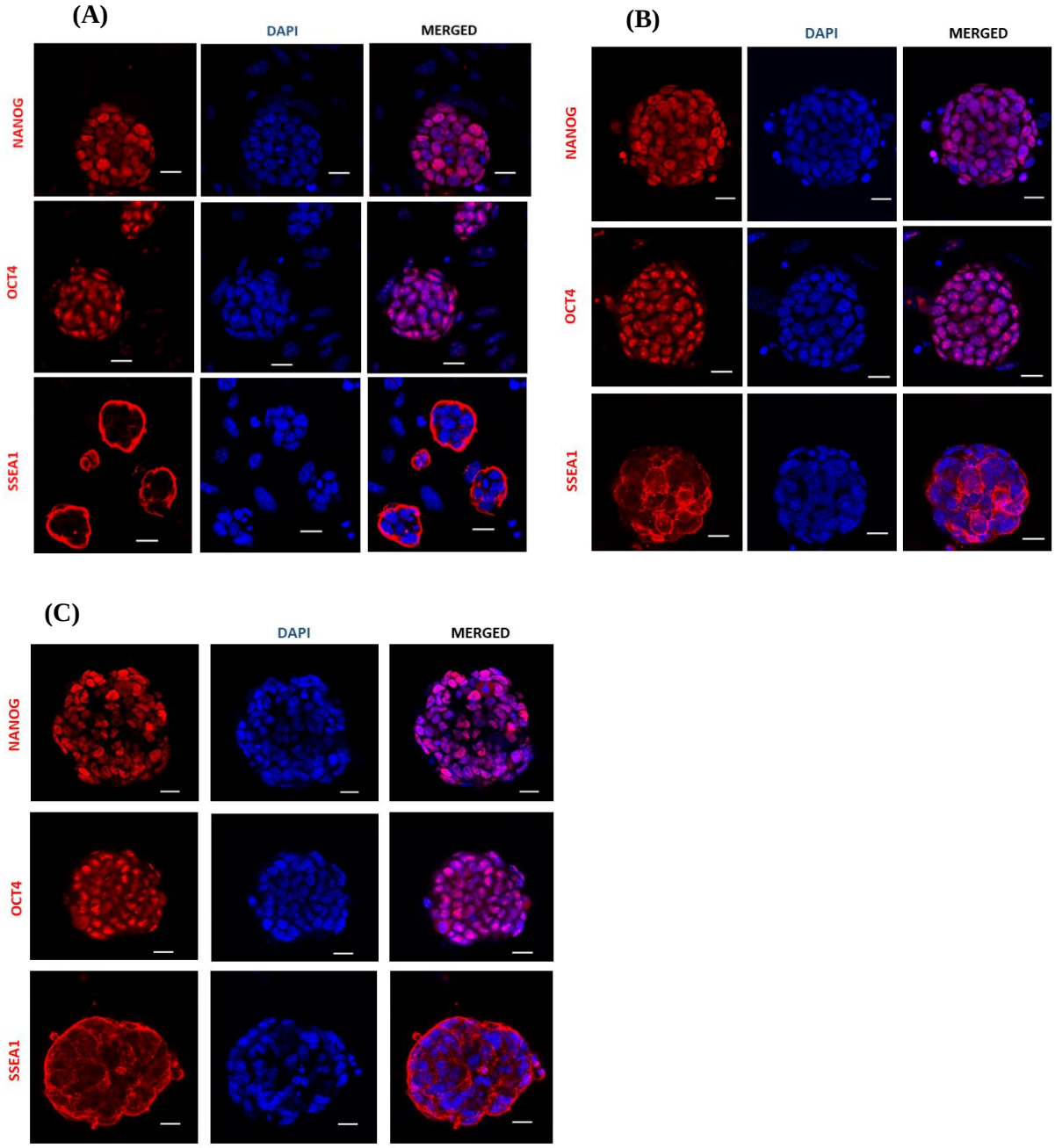

Figure 4.6: Expression of NANOG, OCT4 and SSEA-1 in *Cerl2*$^{-/-}$ ES cells. Immunofluorescence analysis show positive protein expression for the referred regulator markers of pluripotency in mouse *Cerl2*$^{-/-}$ ES cells derived from: (A) Embryo 1; (B) Embryo 5; (C) Embryo 6. Scale bars: 20 µm.

It is notable a significant statistical difference between the relative gene levels for the mouse fibroblasts compared with the *Cerl2*$^{-/-}$ ES cells from all the embryos (Figure 4.7). These results were the expected because mouse fibroblast cells do not express these pluripotency genes. Relatively to the derived cells, all the three lines show comparable or slight higher expression levels compared with the ES cells control for all the endogenous pluripotency genes (Figure 4.7). This could be explained by existence of minor genetic and epigenetic variations of the embryos from ES cell lines were derived or, even, slight alterations during culturing (Allegrucci & Young, 2006). Despite of the protocol standardization, during the first steps of ES cells' derivation, even a small variation in temperature, CO_2 values or disturbance of the plates could lead to differences during the establishment of the cell lines.

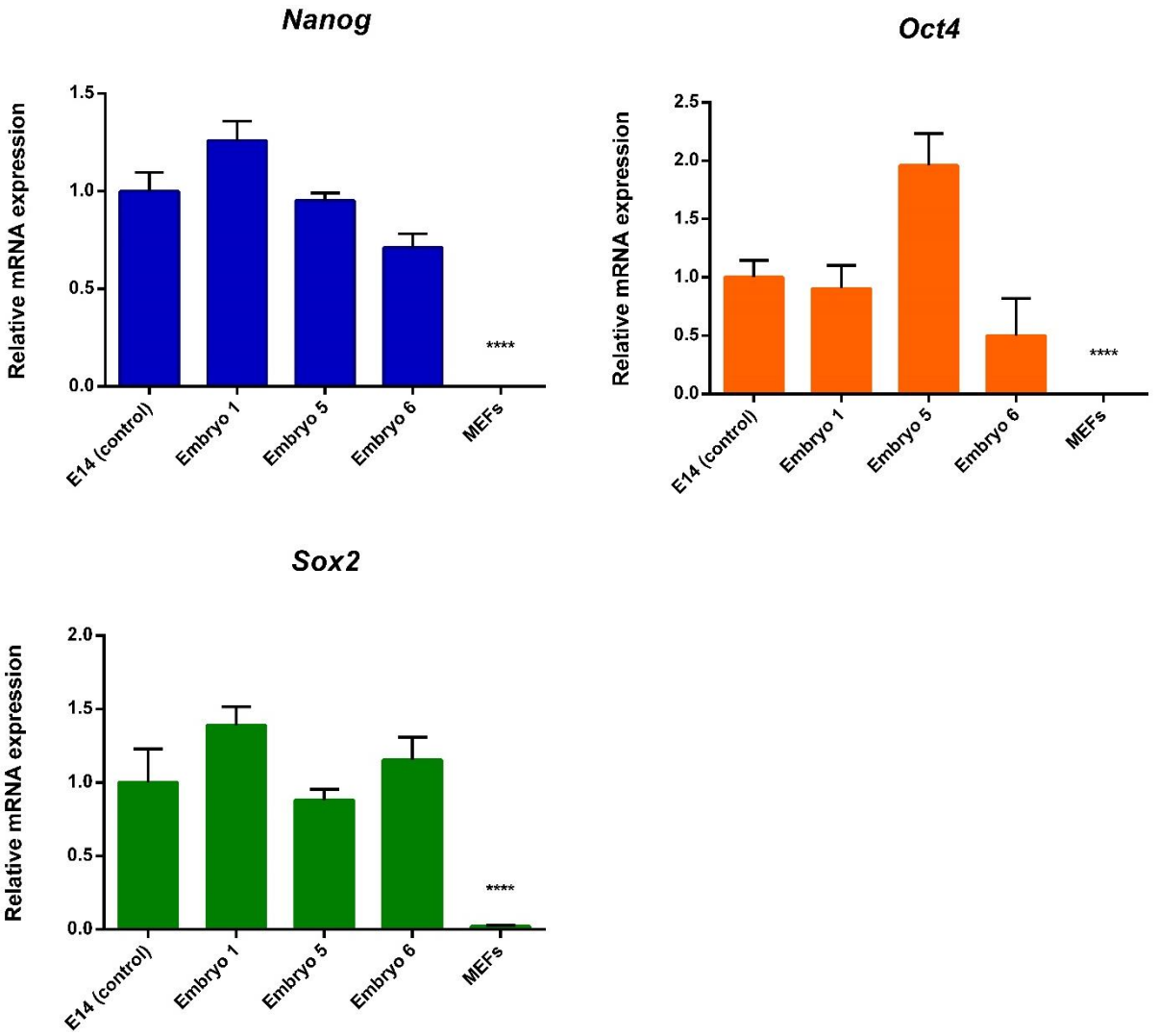

Figure 4.7: Relative expression of *Nanog*, *Oct4* and *Sox2* of the derived mouse *Cerl2*$^{-/-}$ ES cells by qRT-PCR. Samples were collected from *Cerl2*$^{-/-}$ ES cells of the three lines at P6 and the qRT-PCR experiments were performed in triplicate for each one. The expression level of each pluripotency gene is represented relative to the referred E14 ES cell line, used as a positive control. The one-way ANOVA test was used to compare the means of the various cell lines and statistical significant differences where considered when ****P<0.0001.

4.2.3 Spontaneous Differentiation Capacity into the Three Germ Layers

Test the capacity of spontaneous differentiation in the three germ layers is a crucial validation step to guarantee the pluripotency properties of the derived mouse *Cerl2*$^{-/-}$ ES cells (Czechanski et al., 2014). To perform this, the cells were prepared in order to form embryoid bodies using the hanging drop technique. During the first two days of the differentiation protocol (D0-D2), in static suspension culture, the *Cerl2*$^{-/-}$ ES cells tend to aggregate to each other's forming a spheroid body composed by several layers of cells. Through cellular signaling, endoderm, mesoderm and ectoderm started to differentiate. In this way, the resulted embryoid bodies show a homogeneity in the morphology shape and size between the same line and compared to the embryoid bodies from the other two lines (Figure 4.8). This is an important issue because significant differences between the size of the embryoid bodies could influence the number and quality of the differentiated cells from the three germ layers or, even, compromise the correct formation of one of them (Weitzer, 2006).

Using immunofluorescence microscopy, the presence of AFP, α-Actinin sarcomeric and Vimentin were examined. The results show clearly the presence of the three mentioned markers, showing that some

cells spontaneous differentiate to the endoderm lineage, positive marked with AFP, while others differentiate to the cardiac lineage, positive marked with α-Actinin sarcomeric, and others differentiate to the ectoderm lineage, positive marked with Vimentin (Figure 4.8). This could be compared with the total number of cells in each montage by the nucleus' staining with DAPI.

Thus, all the three lines show similar capability to differentiate into the lineage derivatives of the three germ layers confirming the second key feature of pluripotency ability – the differentiation in all cell lineages that compose an organism.

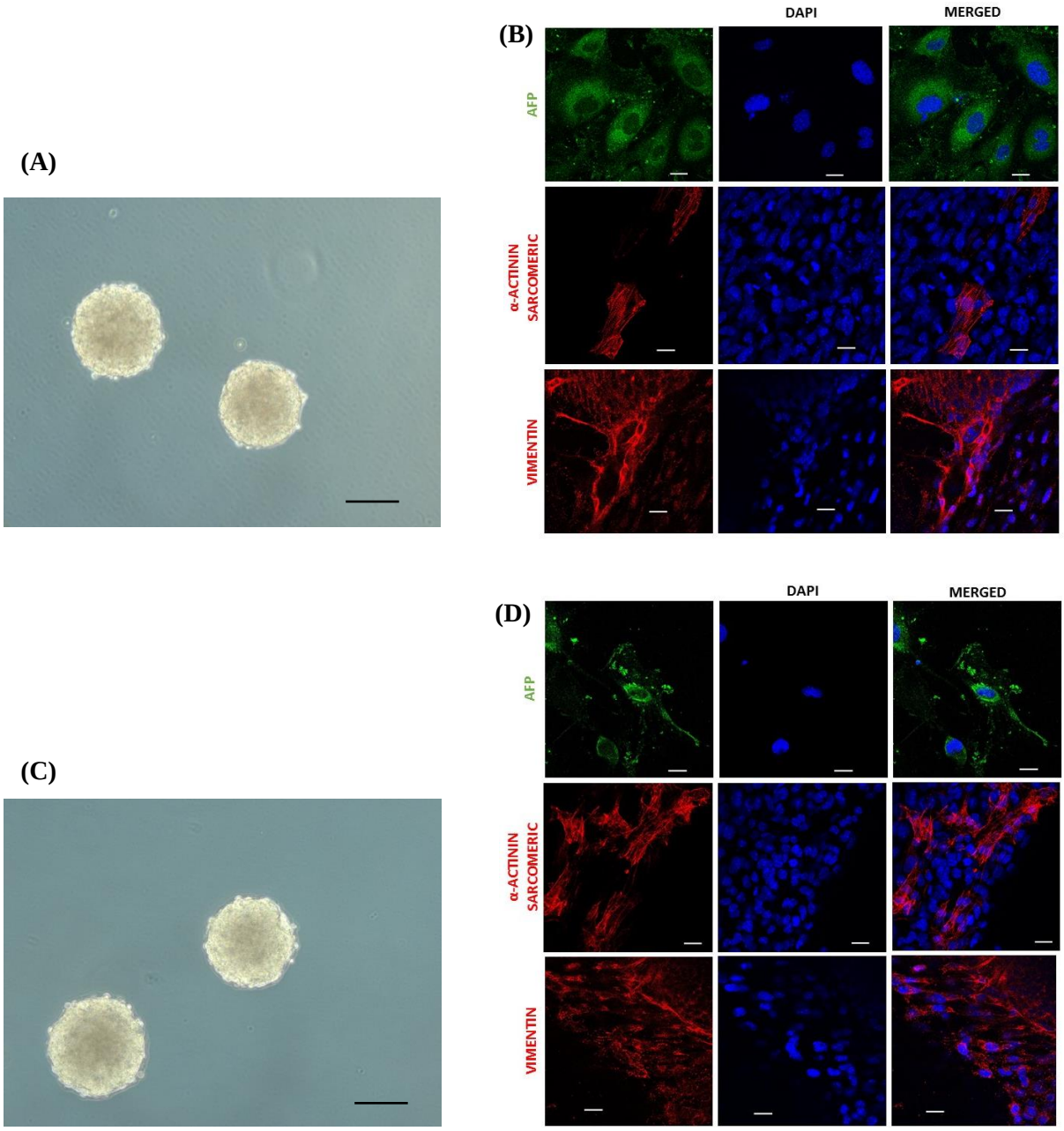

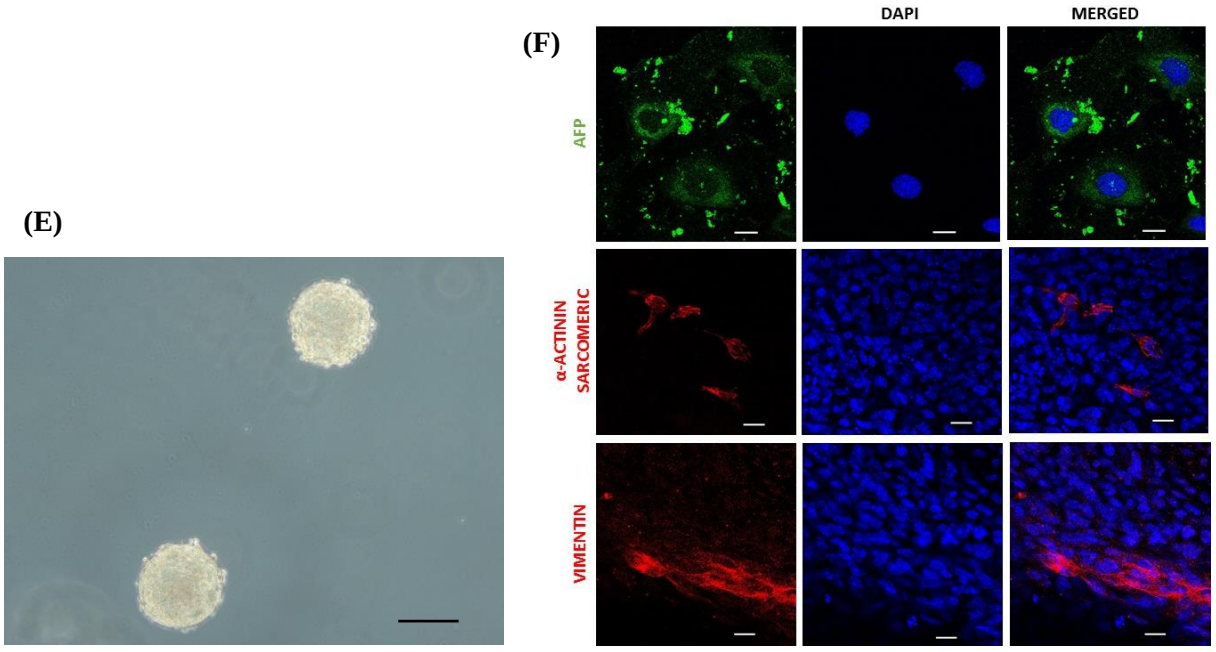

Figure 4.8: Embryoid Bodies, formed from the derived *Cerl2*$^{-/-}$ ES cell lines, differentiate spontaneously into the three germ layers. The ES cells were cultured in suspension and, at day 2 of differentiation, well-developed EBs were formed from: (A) Embryo 1; (C) Embryo 5; and (E) Embryo 6. Scale bars: 100 μm. Then, at day 10 of differentiation, immunofluorescence was performed to the EBs and the presence of AFP (endoderm), α-Actinin sarcomeric (mesoderm) and Vimentin (ectoderm) markers was positively detected from: (B) Embryo 1; (D) Embryo 5; and (F) Embryo 6. Scale bars: 20 μm.

4.3 Differentiation into Cardiomyocytes

After the pluripotency properties and stability of the derived cell lines have been positively proved, they could be used as a reliable model to study the role of Cerl2 behind cardiomyogenesis *in vitro*. Before the implementation of the protocol for cardiac differentiation, it was necessary to reduce the concentration of the MEK and GSK3 inhibitors used in the culture medium supplementation. This occurred as a gradually reduction process, along various passages of the *Cerl2*$^{-/-}$ ES cells, to allow the progressively adaptation of the cells to less amounts of the inhibitors and reduce the likelihood of abrupt differentiation. So, in each passage, the concentration amounts of the 2i were reduced by half the previous concentration value used. Then, *Cerl2*$^{-/-}$ ES cells were maintained in culture only with LIF supplementation to prevent spontaneous differentiation. The described system was chosen in order to avoid the possibility of extension of the Wnt and other signaling pathways, that mediate the pluripotency stage, during the differentiation protocol. Recently, it was demonstrated that when mouse pluripotent cells are cultured in the 2i system for prolonged time, their epigenetic and genomic stability undergoes irreversible changes leading to commitment of their normal development potential (Choi et al., 2017). Consequently, this was carefully considered during the design of the differentiation experiments and the two chemical inhibitors were used only for short-period of time.

The cardiac differentiation experiments were performed only for one *Cerl2*$^{-/-}$ ES cell line in parallel with the WT ES cell line (E14). The KO ES cells derived from Embryo 1 were the chosen ones to serve as the *in vitro* disease model taking in consideration the following motives: it is a male gender line, commonly preferred in studies of gene targeting, because of the presence of all the existing chromosomes in the mouse species; and it demonstrate to have better colonies' morphology, under an inverted microscope, along various passages (Shah et al., 2014). Before starting the cardiac differentiation studies, both KO and WT ES cells were maintained and passaged at least twice without 2i supplementation. The morphology was daily monitored and it was verified a slight pointy change in

the KO colonies' boundaries compared to the morphology shown during initial derivation steps as well as some uncontrolled differentiation events (Figure 4.9). The differentiated cells could be distinguished from the compacted ES cell' colonies by looking for its elongated morphology and single position. However, this was expected according to a lower native pluripotent stage caused by the withdrawal of the 2i chemicals.

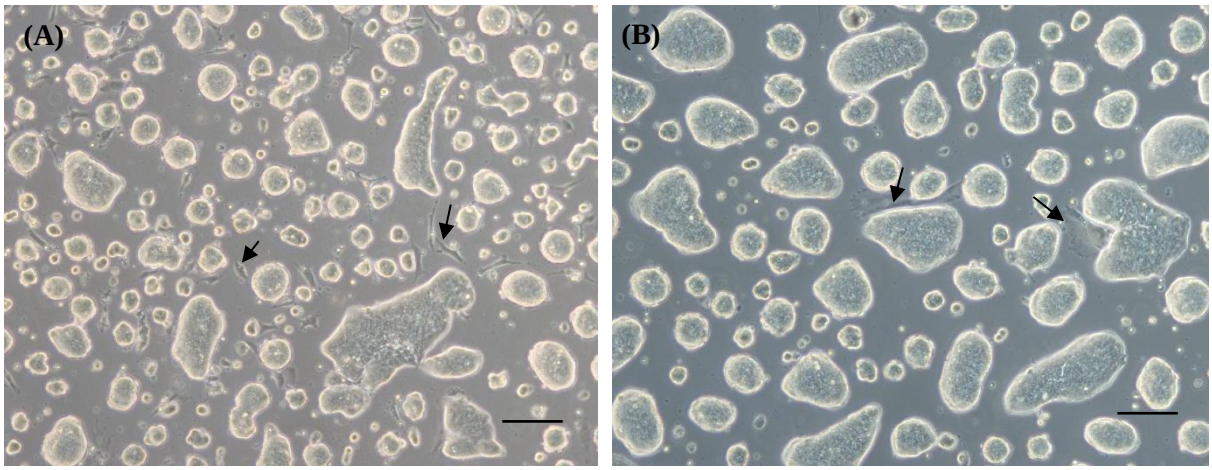

Figure 4.9: Morphology of: (A) KO and (B) WT ES cell lines at day 0 of the differentiation protocol. The ES cells at this stage were cultured without 2i supplementation, showing some events of spontaneous differentiation represented by the black arrows. However, this was a normal consequence of the progressively adaptation of the cells to the absence of the chemical inhibitors. Scale bars: 100 μm.

The differentiation of pluripotent KO and WT cells into mature cardiomyocytes was induced by the hanging drop method leading to the Embryoid Bodies' formation. This protocol was performed in three independent experiments. Through a spontaneous differentiation process, along 10 days, cardiac cells were originated with observable rhythmic beating foci. Firstly, cells' suspension without LIF was pipetted in a specific and comparable concentration (500 cells per drop) in each Petri dish for the KO and WT ES cell lines. Within 48 hours, ES cells were capable to aggregate in 3D structures through stochastic events stimulated by the gravity effect (Figure 4.10) (Kurosawa, 2007). Then, the formed EBs were maintained in suspension culture until day 5 of differentiation, to allow its size growing, to stimulates the specific differentiation of their cell layers into each specific germ layer lineage and, consequently, leads to their surface smoothness. The evolution on size and shape of EBs were daily monitored in order to control the progression of the differentiation protocol and discard cases in which two or more EBs tend to aggregate when too close together, forming a single deformed and large structure. This constant control is decisive because when this occur, the abnormal EBs did not proliferate and differentiate as expected and cell's death phenomena are increased (Rungarunlert et al., 2009). With a reduction in the EBs viability, apoptosis signals are released and could induce slightly changes in the neighbor EBs affecting the efficiency of cardiomyogenesis (Rungarunlert et al., 2009).

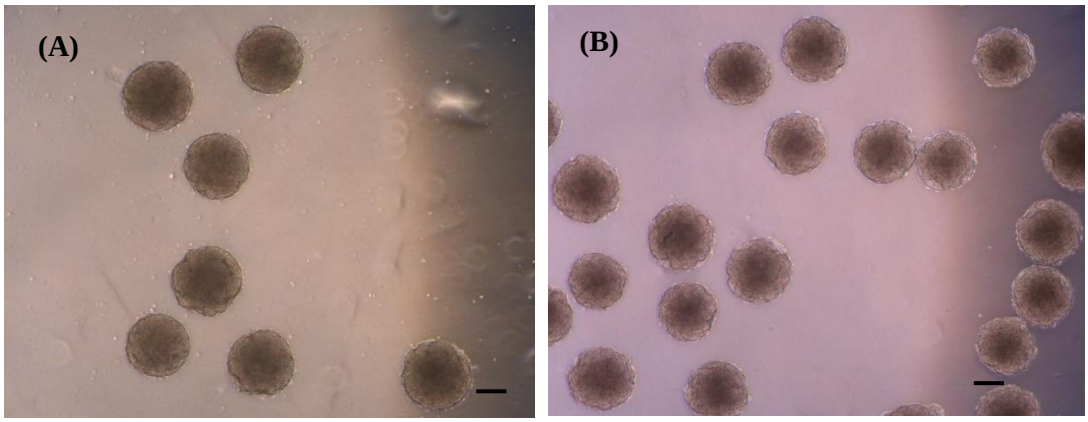

Figure 4.10: Morphology of the derived: (A) KO and (B) WT EBs at day 2 of the differentiation protocol. All the EBs showed a round shape, with irregular surface protrusions. Scale bars: 100 μm.

At day 5 of differentiation, the KO and WT EBs were plated onto gelatin-coated 6-well plates. In each well, an equal number of EBs were plated to perform a normalized comparison between cardiac mesoderm differentiation capacity from the KO and the control lines. Once again, the adherence and cells' spread to the plate' surfaces were monitored every day. During days 6-10, it was notorious a significant difference in the adhesion capacity between the EBs derived from the KO and the control lines (Figure 4.11). In the case of the *Cerl2* mutants, the rate of cells' adhesion was higher and it was observable that the EBs' bodies do not disperse in the plate's surface as much as the control ones (Figure 4.11 – A). They continue to grow, until the end of the protocol, mainly as a compact body with slightly regions composed by dispersed cell' layers.

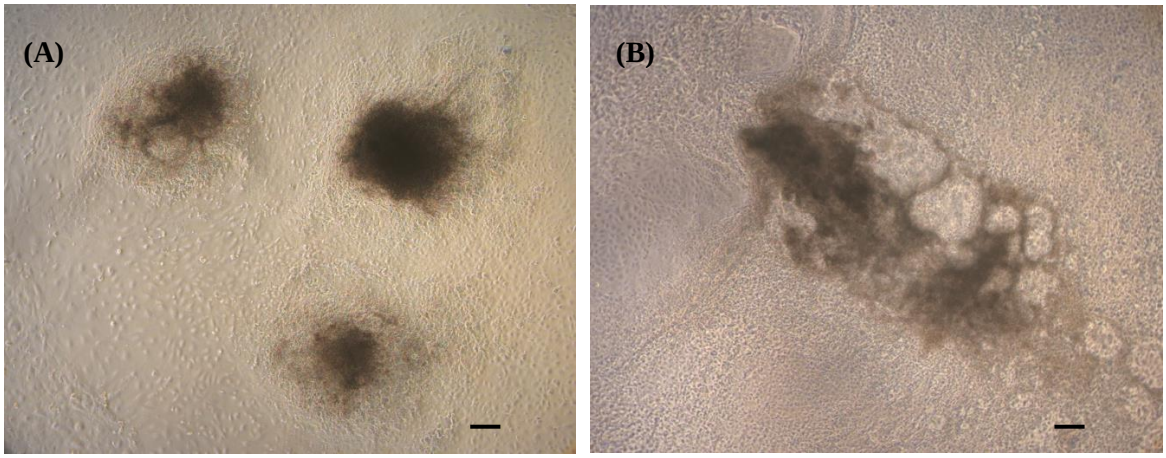

Figure 4.11: Morphology of: (A) three KO EBs and (B) one WT EB at day 10 of the differentiation protocol. It is notorious a significant difference in the adhesion capacity between the mutant and the control lines. Scale bars: 100 μm.

Interestingly, beating foci areas started to be prior visible in the KO differentiated cells. At day 6, their contractile movements were notorious in all the plated EBs at different rhythmic rates, like as *in vivo* (Wobus et al., 1991). In the case of the control line, the beating foci areas start to show contractile movements only between day 7 and day 8 in sporadic number of EBs. From day 6 until day 10 of the differentiation, the number of beating foci were counted, under an inverted microscope, for the KO and WT lines.

In the three cardiac differentiation experiments were observed the same mentioned alterations between the KO and WT cells. Performing the statistical analysis to the counted contractile areas, it was revealed that each KO EB originates the double of beating foci areas compared to the WT EBs along the entire

differentiation protocol (Figure 4.12). Between day 7 and day 10, the median differences were statistically significant between the two cell lines, indicating that from the initial to the final stages of differentiation the mutant *Cerl2* cells shows a higher capacity to develop beating foci areas. This effect indicates that the loss-of-function of the *Cerl2* gene promotes the event of cardiomyocytes formation leading to an increase in cardiac rhythmic areas that could be explained by the high number of mature cardiac cells, compared to the control line. Also, it appears that the signaling pathways involved in cardiac fate may be overstimulated leading to an early mesoderm differentiation. It would be possible that this rapid specification of the cardiac mesoderm could influence the number and electrophysiological abilities of the cardiac progenitors and mature cardiomyocytes. So, with the purpose to investigate if expression levels of mesoderm genes are raised and study their evolution expression during the differentiation protocol, RNA samples were extracted every 48 hours from the differentiating KO and WT EBs. Then, cDNA was synthesized and used as template for quantitative RT-PCR experiments. Cardiac specific genes, including *Mesp-1*, *Isl1*, *Nkx2.5*, *α-MHC* and *cTnT*, were assayed as markers to study the cardiac differentiation and specification along time (Meilhac et al., 2014).

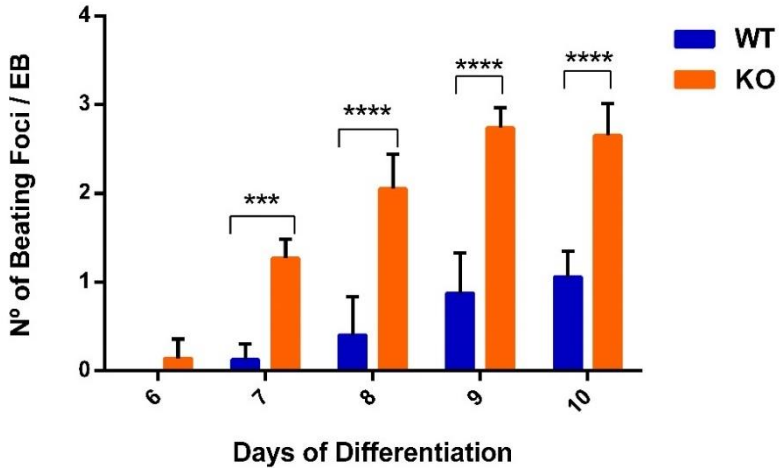

Figure 4.12: Measurement of beating foci per KO and WT EBs. Results are expressed as the total number of beating foci with respect to the total number of plated EBs and represent the mean ± SD of three independent experiments. Unpaired Student's t-test was applied to compare the differences between WT and KO groups in each day of differentiation. Statistical significant results were considered when ***P<0.001 and ****P<0.0001.

Firstly, to confirm that *Cerl2* is not expressed during the KO ES cells differentiation, the quantitative RT-PCR was performed for this gene. As expected, no levels of expression were found in the mutant cells. Also, the resulting data was relevant to study the peak day of normal expression of this gene relating to the *in vivo* mechanism. It is known that Cerl2 started to be asymmetrically expressed in the right side of the mouse node, continuing its dynamically signal translocation in association to the Nodal pathway (Inácio et al., 2013). These events occur at the LPM development during the first phases of cardiogenesis. So, it was expected that around day 4 of differentiation, levels of *Cerl2* reach their peak in the control line (Figure 4.13 – A). After day 4 of differentiation, levels of Cerl2 expression start to reduce and a second upregulation is notorious between days 8-10. Considering that during this time window, cardiomyocytes start to differentiate into specific cardiac lineages, Cerl2 could be recruited to regulate the pathways involved in proliferation and specification of cardiomyocytes. One of them is the Wnt/β-catenin canonical signaling pathway, implicated in early cardiovascular development (Buikema et al., 2013). In a previous work, it was reported the interaction between Wnt signaling pathway and *Cerl2* in the first steps of L-R asymmetry: an interacting feedback loop between Wnt and *Cerl2* is responsible for the generation of the signal asymmetry at the mouse node and, also, Cerl2 is capable to

inhibit the Wnt self-activating loop (Nakamura et al., 2012). Thus, in view of the second increase in Cerl2 levels it may be possible that Wnt pathway and Cerl2 could be connected again during the cardiac cells proliferation.

Relative *Mesp-1* mRNA expression was found in the EBs at day 4 of differentiation, in both lines. The high levels of expression are consistent with the period of cardiac mesoderm formation. When correlated to the *in vivo* cardiogenesis, Mesp-1 proteins start to be recruited to the mouse primitive streak at E6.5 (Meilhac et al., 2014). Its expression is observed transiently during the phase of mesoderm formation, consequently marking all the cardiac progenitors regardless of their future lineage specification (Meilhac et al., 2014). It was found that the KO cells show a statistically significant higher level of *Mesp-1* expression, relatively to the WT cells (Figure 4.13 – B). This data suggests that in the absence of *Cerl2*, ES cells demonstrated to have an increased capacity for mesoderm formation towards the *Mesp-1* cardiogenic mesoderm lineage. Also, it suggests the production of a higher number of cardiac progenitors by the *Cerl2*$^{-/-}$ ES cells, resulted in a superior number of *Mesp-1* mRNA templates available during the reactions of amplification in real-time. The quickly amplification leads to lower Ct values resulting in higher levels of relative *Mesp-1* expression for the KO EBs.

The First Heart Field progenitors can be identified through the positive expression marker of *Nkx2.5* gene. This first cardiac lineage contributes primarily to the formation of the linear heart tube and ultimately to the origin of the mature cardiac cells that will populate the left ventricle (Buckingham et al., 2005). This heart chamber can be structurally and morphologically affected by slightly perturbances in the normal development of the FHF cell lineage. Prior investigations demonstrated the myocardium enlargement of the left ventricle walls in the *Cerl2* KO mice caused by cardiomyocytes' hyperplasia (Araújo et al., 2014). Correlating these facts, it would be possible that an increase of the *Nkx2.5* expression during mouse cardiogenesis could coincide with the origin of a higher number of FHF progenitors capable to form a robust myocardium tissue, comparatively to control levels. Indeed, in the quantitative RT-PCR results, *Nkx2.5* is upregulated in the differentiated *Cerl2*$^{-/-}$ ES cells (Figure 4.13 – C). At day 6, its levels increased significantly marking the stage of cells' commitment into the first myocardial lineage. In addition, levels of *Isl1* expression increased substantially at day 4, reaching the peak at day 6 for the mutant and the control lines. Second Heart Field cells are often identified by the positive expression of *Isl1* being these cells the late cardiac progenitors for myocardial, endothelial and smooth muscle cells (Moretti et al., 2006). Comparing the relative levels of *Isl1* expression at day 6, the differentiation of *Cerl2*$^{-/-}$ ES cells leads to statistically higher levels of gene expression compared to the control line (Figure 4.13 – D). Once again, these results corroborate the hypothesis that loss-of-function of *Cerl2* gene increases proliferation of cardiomyocytes explained by a higher production of SHF progenitor cells. Curiously, it is verified that even in the last days of differentiation relative *Isl1* expression was maintained in similar high levels. This could be an indicator of an incomplete mechanism of cardiomyocytes' differentiation and, consequently, their phenotypic maturation could be affected.

Then, to investigate the functionality state of cardiomyocytes' maturation, levels of *α-MHC* and *cTnT* expression were quantified. Myosin is the principal protein that contribute to the generation of the contractile movements during heart function, through mediation of ATP molecules (Ng et al., 2010). Among its constituent elements, its structure is composed by two myosin heavy chains (MHC). During the early mouse development, the expression of α-MHC start to be evident in the cardiac crescent with progressing augmented levels throughout the heart tube structure (Brade et al., 2013). Considering the qRT-PCR results, it was identified a significant alteration for the *α-MHC* gene expression since day 6 until day 10 of the differentiation protocol (Figure 4.13 – E). It is evident a statistical difference between the relative expression levels of the two differentiated cell lines, mainly at day 10: the *Cerl2*$^{-/-}$ cardiomyocytes revealed upregulation of this structural protein. This data could be a consequence of an intensified stimulation of KO cardiomyogenesis resulted from the loss-of-function of Cerl2. On the other

hand, it is known that cTnT is one of the principal regulatory proteins capable to control the ionic Ca^{2+} variations and anchor the other troponin components, essential for myocardium contraction (Nishii et al., 2008). Also, its roles are related to the assembly of sarcomeres' structure capable to influence the systolic and diastolic functions (Tardiff et al., 1999). Analysis of the *cTnT* expression revealed decreased levels in the differentiated *Cerl2*$^{-/-}$ ES cells at day 10, comparatively with the WT cells (Figure 4.13 – F). The results indicate a possible structural commitment of the derived *Cerl2*$^{-/-}$ cardiomyocytes characterized by a reduced number of cTnT proteins at the sarcomeres level. This is in agreement with prior results that demonstrated a decrease in *cTnT* expression in the mutant mouse embryos at E13 and E15 (Araújo et al., 2014).

Previously, cyclins and cyclin-dependent kinase (CDKs) were defined as regulatory molecules during embryonic cardiomyocytes division (Ikenishi et al., 2012). During this development process, it was reported that the Wnt/β-catenin pathway is capable to interfere in the proliferation capacity, mainly in the ventricular cardiomyocytes (Buikema et al., 2013). The recruitment of Ccnd1 and Ccnd2 (Cyclin D1 and Cyclin D2) proteins is one of the key source of the cardiac cell cycle. With the purpose to study if there is a change in the number of mitotic events, levels of *Ccnd1* were tested. Only this cell cycle regulator was tried, considering that in previous results only upregulated levels of *Ccnd1* were found in left ventricular cardiomyocytes from the mutant Cerl2 neonatal mice (Araújo et al., 2014). In the present data, a statistical increase of *Ccnd1* was only found in the *Cerl2*$^{-/-}$ cells at day 10 (Figure 4.13 – G). An increase in *Ccdn1* expression in the differentiated *Cerl2*$^{-/-}$ ES cells could explain the high number of derived-cardiomyocytes. Perhaps, the Wnt signaling pathway is altered in the absence of Cerl2 proteins demonstrated by the increased in *Ccdn1* expression levels, considering that is one of its target genes.

Furthermore, to confirm the present data, it will be necessary to perform Flow Cytometry experiments to the differentiated *Cerl2*$^{-/-}$ ES cell populations. Using this technique, it is possible to have a reliable quantitative result related to the number of derived cardiac progenitor cells and cardiomyocytes. However, due to time issues it was not possible to perform these experiences in order to confirm the results obtained so far.

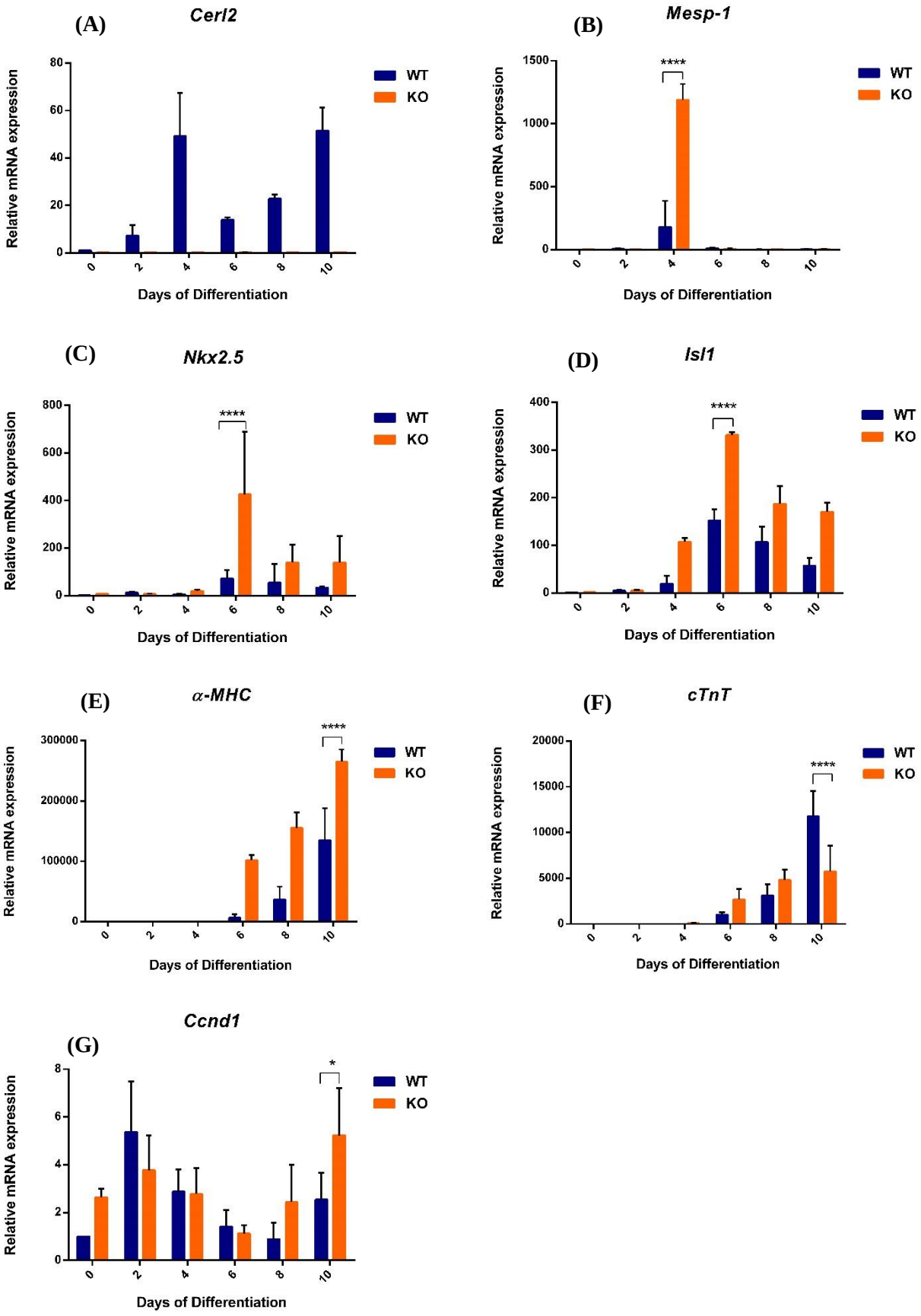

Figure 4.13: Relative mRNA expression of cardiac genes in *Cerl2*$^{-/-}$ and WT differentiated cells. qRT-PCR experiments were performed in triplicate for (A) *Cerl2*, (B) *Mesp-1*, (C) *Nkx2.5*, (D) *Isl1*, (E) *α-MHC*, (F) *cTnT*, (G) *Ccnd1*. Results are represented as mean ± SD of three independent biological experiments. Unpaired Student's t-test was applied to compare the

differences between WT and KO groups in each day of differentiation. Statistical significant results were considered when *P<0.05 and ****P<0.0001.

5. Conclusions and Future Perspectives

The generation of cardiomyocytes through differentiation of ES cells demonstrate to have several applications in the scientific field. During the last decades, mutant ES cells have been used as disease models to study specificities and uncover the biological mechanisms that lead to the origin of congenital heart diseases (Habib et al., 2008) (Dambrot et al., 2011). Exploring their abilities to differentiate in all the cell lineages of the mammalian organism, it is possible to mimic *in vitro* the first stages of embryogenesis and follow important molecules. One of the central step is the establishment of the L-R asymmetric morphogenesis of the organs, which will influence the subsequent mechanisms during cardiogenesis.

The *Cerl2* gene, member of the *Cerberus/Dan* family, encodes for a protein capable to regulate Nodal with an important role in the L-R axis establishment (Marques et al., 2004). The proper positioning of the heart and great vessels in the rib cage is intimately dependent of its regulation activity on Nodal signaling pathway. When loss-of-function of *Cerl2* is verified, the resulted mutant phenotype is described by congenital laterality disorders (Marques et al., 2004). Previously, studies performed in *Cerl2*$^{-/-}$ mice demonstrated that these animals have a compromise in cardiac electrophysiology with an associated significant mortality rate within a few hours after birth (Araújo et al., 2014) (Marques et al., 2004). Also, an enlargement on the ventricular walls was observed allied with an increase in mitotic index of cardiomyocytes.

In the present Dissertation, with the purpose to discover if Cerl2 is involved in the mechanisms that control proliferation and differentiation of cardiomyocytes during the first stages of life, three *Cerl2*$^{-/-}$ ES cell lines were derived and characterized to serve as a heart disease model. For this, blastocysts were collected from the *Cerl2* knockout mice after three days of pregnancy. Performing the standard protocols, it was demonstrated that the derived lines show a stable karyotype, are capable to maintain unlimited capacity to self-renew, by expression of *Nanog*, *Oct4*, *Sox2* and *SSEA1* pluripotency genes, and can originate the three primordial germ layers. Then, the hypothesis of alteration in cardiac mesoderm induction was tested using the protocol of EBs formation to differentiate the *Cerl2*$^{-/-}$ ES cells. During the differentiation experiments, it was observed an early appearance of beating foci areas in a high number, compared to the control line. Also, in the mutant cells, the adhesion capacity was compromised showed by the compact growing of the EBs through the culture plate surface. These results demonstrate that mesoderm differentiation is overstimulated resulting in the early appearance of contractile areas associated with an increased number of them. Also, the obvious increase in adhesion capacity could be caused by this rapid cardiac mesoderm formation that could influence the differentiation capability of endoderm or ectoderm. Taking into account that primitive endoderm is the first cells' layer of the EBs to attached and spread to the plate surface, it could be possible that this germ layer is the most compromised. In future work, it will be important to perform immunofluorescence tests to check E-cadherin expression. Using this marker, it will be possible to investigate if cell-cell adhesion, proliferation and/or mobility are altered during germ layers' differentiation (Maître & Heisenberg, 2013).

Concerning the expression of cardiac genes during the *Cerl2*$^{-/-}$ ES cells differentiation, it was observed an upregulation of *Mesp-1*, *Isl1* and *Nkx2.5*. Once again, these data demonstrate that cardiac mesoderm differentiation is highly stimulated in case of *Cerl2* loss-of-function. Also, the high levels of relative *Isl1* and *Nkx2.5* expression revealed that the production of cardiac progenitors, derived from the First and Second Heart Fields, could be increased. The upregulation of *Nkx2.5*, at day 6 of differentiation, is a suggestion of a high number of FHF progenitors that could explain the robust myocardium of the left ventricles' walls observed in the *Cerl2*$^{-/-}$ mice. Also, alterations in levels of expression of genes essential for proper cardiomyocytes contraction (*α-MHC* and *cTnT*) were observed. If the loss-of-function of *Cerl2* leads to an increase in production of cardiac progenitor cells, it will be expected that more mature cardiomyocytes are produced. Indeed, high levels of relative *α-MHC* expression were detected in the knockout cells leading to the possibility of a high number of derived-cardiomyocytes. However, decreased levels of *cTnT* expression were found in the differentiated *Cerl2*$^{-/-}$ ES cells. These data indicate that the produced cardiomyocytes were not fully mature possible resulted from a commitment in cTnT proteins that compose their sarcomeres structure. A statistical significant difference was observed, at day 10 of differentiation, for levels of *Ccdn1* expression between the mutant and the control lines. An increase in *Ccdn1* expression in the differentiated *Cerl2*$^{-/-}$ ES cells could explain the high number of derived-cardiomyocytes. According to the cell cycle regulator role of *Ccdn1*, its upregulation could be translated in a high number of mitotic divisions for cardiomyocytes (Ikenishi et al., 2012). Still, *Ccdn1* is one of the Wnt canonical signaling target genes, being this pathway involved in early cardiovascular development (Buikema et al., 2013). Perhaps, the Wnt signaling pathway is altered in the absence of Cerl2 proteins demonstrated by the increased in one of its target molecules. In order to clearly prove that the loss-of-function of *Cerl2* leads to an improvement in the cardiomyocytes production, it is crucial to analyze, in the future, the differentiated *Cerl2*$^{-/-}$ ES cell populations using Flow Cytometry experiments. Using this technique, it is possible to have a reliable quantitative result related to the number of derived cardiac progenitor cells and cardiomyocytes. In addition, it will be relevant to perform proliferation assays to assess the proliferation capacity of the *Cerl2*$^{-/-}$ derived-cardiomyocytes by performing a BrdU labelling assay.

This project also revealed the normal temporal changes in the expression levels of *Cerl2* throughout the cardiac differentiation protocol. In the control line, the differentiated ES cells demonstrated a high expression of *Cerl2* at day 4, corresponding to the *in vivo* stage when its proteins are recruited to direct Nodal proteins and maintain the normal Nodal flow during the L-R axis patterning. Still, it was notorious a second upregulation at the end of the differentiation protocol. This data could indicate that Cerl2 is also promoted to regulate cardiac lineage fate and proliferation. A previous study reported feedback loops interlinking the Wnt signaling pathway and *Cerl2* capable to generate together the L-R asymmetry at the mouse node and revealed the capacity of Cerl2 in inhibition of the Wnt self-activating loop (Nakamura et al., 2012). Thus, in view of the second increase in Cerl2 levels it may be possible that Wnt pathway and Cerl2 could be connected during the cardiac cells proliferation. In the case of mutation in the *Cerl2* gene, Wnt signaling pathway could be prolonged also explained by the increased levels of *Ccdn1*. However, further experiments need to be performed to confirm the possible role of Cerl2 as a regulator of Wnt canonical signaling.

As final conclusions, the present Dissertation uncovers the first insights related to the *Cerl2* role as a possible regulator of the mechanisms involved in specification of the produced number of cardiac cells during mouse cardiomyogenesis.

References

Allegrucci, C., & Young, L. E. (2006). Differences between human embryonic stem cell lines. *Human Reproduction Update*, *13*(2), 103–120.

Araújo, A. C., Marques, S., & Belo, J. A. (2014). Targeted inactivation of cerberus like-2 leads to left ventricular cardiac hyperplasia and systolic dysfunction in the mouse. *PLoS ONE*, *9*(7), 1-12.

Aubert, J., Dunstan, H., Chambers, I., & Smith, A. (2002). Functional gene screening in embryonic stem cells implicates Wnt antagonism in neural differentiation. *Nature Biotechnology*, *20*(12), 1240–1245.

Avilion, A. A., Nicolis, S. K., Pevny, L. H., Perez, L., Vivian, N., & Lovell-Badge, R. (2003). Multipotent cell lineages in early mouse development on SOX2 function. *Genes Dev.*, *17*, 126–140.

Bai, F., Ho Lim, C., Jia, J., Santostefano, K., Simmons, C., Kasahara, H., Wu, W., Terada, N., & Jin, S. (2015). Directed Differentiation of Embryonic Stem Cells Into Cardiomyocytes by Bacterial Injection of Defined Transcription Factors. *Scientific Reports*, *5*(15014), 1-19.

Batlle-Morera, L., Smith, A., & Nichols, J. (2008). Parameters influencing derivation of embryonic stem cells from murine embryos. *Genesis*, *46*(12), 758–767.

Beddington, R. S. P., & Robertson, E. J. (1999). Axis development and early asymmetry in mammals. *Cell*, *96*(2), 195–209.

Belo, J. A., Silva, A. C., Borges, A. C., Filipe, M., Bento, M., Gonçalves, L., Vitorino, M., Salgueiro, A., Teixeira, V., Tavares, A. T., & Marques, S. (2009). Generating asymmetries in the early vertebrate embryo : the role of the Cerberus-like family. *International Journal of Developmental Biology*, *53*, 1399–1407.

Bergmann, O., Bhardwaj, R. D., Bernard, S., Zdunek, S., Barnabé-Heider, F., Walsh, S., Zupicich, J., Alkass, K., Buchholtz, B. A., Druid, H., Jovinge, S., & Frisén, J. (2009). Evidence for cardiomyocyte renewal in humans. *Science*, *324*(5923), 98–102.

Bergmann, O., Zdunek, S., Felker, A., Salehpour, M., Alkass, K., Bernard, S., Sjostrom, S. L., Szewczykowska, M., Jackowska, T., dos Remedios, C., Malm, T., Andrã, M., Jashari, R., Nyengaard, J. R., Possnert, G., Jovinge, S., Druid, H., & Frisén, J. (2015). Dynamics of Cell Generation and Turnover in the Human Heart. *Cell*, *161*(7), 1566–75.

Bickmore, W. A. (2001). Karyotype Analysis and Chromosome Banding. In Nature (Ed.), *Encyclopedia of Life Sciences* (pp. 1–7). Chichester, UK: John Wiley & Sons, Ltd.

Boheler, K. R., Czyz, J., Tweedie, D., Yang, H. T., Anisimov, S. V., & Wobus, A. M. (2002). Differentiation of pluripotent embryonic stem cells into cardiomyocytes. *Circulation Research*, *91*(3), 189–201.

Bolli, R., Chugh, A. R., D'Amario, D., Loughran, J. H., Stoddard, M. F., Ikram, S., … & Anversa, P. (2011). Cardiac stem cells in patients with ischaemic cardiomyopathy (SCIPIO): initial results of

a randomised phase 1 trial. *The Lancet*, *378*(9806), 1847–1857.

Bondue, A., Lapouge, G., Paulissen, C., Semeraro, C., Iacovino, M., Kyba, M., & Blanpain, C. (2008). Mesp1 acts as a master regulator of multipotent cardiovascular progenitor specification. *Cell Stem Cell*, *3*(1), 69–84.

Bouwmeester, T., Kim, S., Sasai, Y., Lu, B., & De Robertis, E. M. (1996). Cerberus is a head-inducing secreted factor expressed in the anterior endoderm of Spemann's organizer. *Nature*, *382*(6592), 595-601.

Brade, T., Pane, L. S., Moretti, A., Chien, K. R., & Laugwitz, K. L. (2013). Embryonic heart progenitors and cardiogenesis. *Cold Spring Harbor Perspectives in Medicine*, *3*(10), 1-17.

Brand, T. (2003). Heart development: Molecular insights into cardiac specification and early morphogenesis. *Developmental Biology*, *258*(1), 1–19.

Braunwald, E., & Pfeffer, M. A. (1991). Ventricular enlargement and remodeling following acute myocardial infarction: mechanisms and management. *The American Journal of Cardiology*, *68*(14), 1D–6D.

Buckingham, M., Meilhac, S., & Zaffran, S. (2005). Building the mammalian heart from two sources of myocardial cells. *Nature Reviews Genetics*, *6*, 826–835.

Buikema, J. W., Mady, A. S., Mittal, N. V, Atmanli, A., Caron, L., Doevendans, P. A., Sluijter, J. P. G., & Domian, I. J. (2013). Wnt/β-catenin signaling directs the regional expansion of first and second heart field-derived ventricular cardiomyocytes. *Development*, *140*(20), 4165–4176.

Bustin, S. A. (2000). Absolute quantification of mrna using real-time reverse transcription polymerase chain reaction assays. *Journal of Molecular Endocrinology*, *25*(2), 169–193.

Cai, C. L., Liang, X., Shi, Y., Chu, P. H., Pfaff, S. L., Chen, J., & Evans, S. (2003). Isl1 identifies a cardiac progenitor population that proliferates prior to differentiation and contributes a majority of cells to the heart. *Developmental Cell*, *5*(6), 877–889.

Cambria, E., Steiger, J., Günter, J., Bopp, A., Wolint, P., Hoerstrup, S. P., & Emmert, M. Y. (2016). Cardiac Regenerative Medicine: The Potential of a New Generation of Stem Cells. *Transfusion Medicine and Hemotherapy*, *43*(4), 275–281.

Capecchi, M. R. (2005). Gene targeting in mice: functional analysis of the mammalian genome for the twenty-first century. *Nature Reviews. Genetics*, *6*(6), 507–512.

Chambers, I., Colby, D., Robertson, M., Nichols, J., Lee, S., Tweedie, S., & Smith, A. (2003). Functional expression cloning of Nanog, a pluripotency sustaining factor in embryonic stem cells. *Cell*, *113*(5), 643–655.

Choi, J., Huebner, A. J., Clement, K., Walsh, R. M., Savol, A., Lin, K., … & Hochedlinger, K. (2017). Prolonged Mek1/2 suppression impairs the developmental potential of embryonic stem cells. *Nature*, *1*, 1–7.

Chugh, A. R., Beache, G. M., Loughran, J. H., Mewton, N., Elmore, J. B., Kajstura, J., … & Bolli, R. (2012). Administration of Cardiac Stem Cells in Patients With Ischemic Cardiomyopathy: The SCIPIO Trial: Surgical Aspects and Interim Analysis of Myocardial Function and Viability by Magnetic Resonance. *Circulation*, *126*(11_suppl_1), S54–S64.

Cong, L., Ran, F. A., Cox, D., Lin, S., Barretto, R., Hsu, P. D., … & Marraffini, L. A. (2013). Multiplex

Genome Engineering Using CRISPR/VCas Systems. *Science*, *339*(6121), 819–823.

Conlon, F. L., Lyons, K. M., Takaesu, N., Barth, K. S., Kispert, A., Herrmann, B., & Robertson, E. J. (1994). A primary requirement for nodal in the formation and maintenance of the primitive streak in the mouse. *Development*, *120*, 1919–1928.

Coulombe, K. L. K., Bajpai, V. K., Andreadis, S. T., & Murry, C. E. (2014). Heart regeneration with engineered myocardial tissue. *Annual Review of Biomedical Engineering*, *16*, 1–28.

Cristo, F., Inácio, J. M., de Almeida, S., Mendes, P., Martins, D. S., Maio, J., Anjos, R., & Belo, J. A. (2017). Functional study of DAND5 variant in patients with Congenital Heart Disease and laterality defects. *BMC Medical Genetics*, *18*(1), 1-9.

Cui, L. (2004). Spatial Distribution and Initial Changes of SSEA-1 and Other Cell Adhesion-related Molecules on Mouse Embryonic Stem Cells Before and During Differentiation. *Journal of Histochemistry and Cytochemistry*, *52*(11), 1447–1457.

Czechanski, A., Byers, C., Greenstein, I., Schrode, N., Donahue, L. R., Hadjantonakis, A.-K., & Reinholdt, L. G. (2014). Derivation and characterization of mouse embryonic stem cells from permissive and nonpermissive strains. *Nature Protocols*, *9*(3), 559–74.

Czubryt, M. P. (2012). Common threads in cardiac fibrosis, infarct scar formation, and wound healing. *Fibrogenesis & Tissue Repair*, *5*(1), 1-11.

Dambrot, C., Passier, R., Atsma, D., & Mummery, C. L. (2011). Cardiomyocyte differentiation of pluripotent stem cells and their use as cardiac disease models. *The Biochemical Journal*, *434*(1), 25–35.

Davidson, B. P., & Tam, P. P. L. (2000). The node of the mouse embryo. *Current Biology*, *10*(17), 617–619.

Desbaillets, I., Ziegler, U., Groscurth, P., & Gassmann, M. (2000). Embryoid bodies: an in vitro model of mouse embryogenesis. *Experimental Physiology*, *85*(6), 645–651.

Ding, J., Yang, L., Yan, Y. T., Chen, A., Desai, N., Wynshaw-Boris, A., & Shen, M. M. (1998). Cripto is required for correct orientation of the anterior-posterior axis in the mouse embryo. *Nature*, *395*(6703), 702–707.

Doetschman, T. C., Eistetter, H., Katz, M., Schmidt, W., & Kemler, R. (1985). The in vitro development of blastocyst-derived embryonic stem cell lines: formation of visceral yolk sac, blood islands and myocardium. *Journal of Embryology and Experimental Morphology*, *87*, 27–45.

Eisenberg, E., & Levanon, E. Y. (2013). Human housekeeping genes, revisited. *Trends in Genetics*, *29*(10), 569–574.

Evans, M. J., & Kaufman, M. H. (1981). Establishment in culture of pluripotential cells from mouse embryos. *Nature, 292(5819)*, 154-156.

Fallis, A. . (2010). Immunocytochemical Methods and Protocols. *Journal of Chemical Information and Modeling*, *588*(9), 1689–1699.

Fisher, S. A., Doree, C., Mathur, A., & Martin-Rendon, E. (2015). Meta-analysis of cell therapy trials for patients with heart failure. *Circulation Research*, *116*(8), 1361–1377.

Fliegauf, M., Benzing, T., & Omran, H. (2007). When cilia go bad: cilia defects and ciliopathies. *Nature*

Reviews. Molecular Cell Biology, *8*(11), 880–93.

Fujinaga, M. (1997). Development of sidedness of asymmetric body structures in vertebrates. *International Journal of Developmental Biology*, *41*(2), 153–186.

Galdos, F. X., Guo, Y., Paige, S. L., VanDusen, N. J., Wu, S. M., & Pu, W. T. (2017). Cardiac Regeneration. *Circulation Research*, *120*(6), 941–959.

Habib, M., Caspi, O., & Gepstein, L. (2008). Human embryonic stem cells for cardiomyogenesis. *Journal of Molecular and Cellular Cardiology*, *45*(4), 462–474.

Hall, B., Limaye, A., & Kulkarni, A. B. (2009). Overview: Generation of Gene Knockout Mice. *Current Protocols in Cell Biology*, (SUPPL. 44), 1–17.

Hamada, H., Meno, C., Saijoh, Y., Adachi, H., Yashiro, K., Sakuma, R., & Shiratori, H. (2001). Role of asymmetric signals in left-right patterning in the mouse. *American Journal of Medical Genetics*, *101*(4), 324–327.

Hamilton, W. B., & Brickman, J. M. (2014). Erk Signaling Suppresses Embryonic Stem Cell Self-Renewal to Specify Endoderm. *Cell Reports*, *9*(6), 2056–2070.

Hanna, J., Markoulaki, S., Mitalipova, M., Cheng, A. W., Cassady, J. P., Staerk, J., … & Jaenisch, R. (2009). Metastable Pluripotent States in NOD Mouse Derived ES Cells. *Cell Stem Cell*, *4*(6), 513–524.

Harvey, R. P. (1998). Links in the Left / Right Axial Pathway. *Cell Press*, *94*, 273–276.

Ikenishi, A., Okayama, H., Iwamoto, N., Yoshitome, S., Tane, S., Nakamura, K., Obayashi, T., Hayashi, T., & Takeuchi, T. (2012). Cell cycle regulation in mouse heart during embryonic and postnatal stages. *Development, Growth & Differentiation*, *54*(8), 731–738.

Inácio, J. M., Marques, S., Nakamura, T., Shinohara, K., Meno, C., Hamada, H., & Belo, J. A. (2013). The Dynamic Right-to-Left Translocation of Cerl2 Is Involved in the Regulation and Termination of Nodal Activity in the Mouse Node. *PLoS ONE*, *8*(3).

Itskovitz-Eldor, J., Schuldiner, M., Karsenti, D., Eden, A., Yanuka, O., Amit, M., Soreq, H., & Benvenisty, N. (2000). Differentiation of human embryonic stem cells into embryoid bodies compromising the three embryonic germ layers. *Molecular Medicine (Cambridge, Mass.)*, *6*(2), 88–95.

Jeevanantham, V., Butler, M., Saad, A., Abdel-Latif, A., Zuba-Surma, E. K., & Dawn, B. (2012). Adult bone marrow cell therapy improves survival and induces long-term improvement in cardiac parameters: A systematic review and meta-analysis. *Circulation*, *126*(5), 551–568.

Jinek, M., East, A., Cheng, A., Lin, S., Ma, E., & Doudna, J. (2013). RNA-programmed genome editing in human cells. *eLife*, *2013*(2), 1–9.

Johnson, M. H., & Ziomek, C. A. (1981). The foundation of two distinct cell lineages within the mouse morula. *Cell*, *24*(1), 71–80.

Jordan, M. A., & Wilson, L. (2004). Microtubules as a target for anticancer drugs. *Nat. Rev. Cancer*, *4*(4), 253–265.

Kalyan, A., Carneiro, B. A., Chandra, S., Kaplan, J., Chae, Y. K., Matsangou, M., Hendrix, M. J. C., & Giles, F. (2017). Nodal Signaling as a Developmental Therapeutics Target in Oncology. *Molecular*

Cancer Therapeutics, *16*(5), 787–792.

Kamachi, Y., Uchikawa, M., & Kondoh, H. (2000). Pairing SOX off: with partners in the regulation of embryonic development. *Trends in Genetics : TIG*, *16*(4), 182–7.

Karkera, J. D., Lee, J. S., Roessler, E., Banerjee-Basu, S., Ouspenskaia, M. V, Mez, J., … Muenke, M. (2007). Loss-of-function mutations in growth differentiation factor-1 (GDF1) are associated with congenital heart defects in humans. *American Journal of Human Genetics*, *81*(5), 987–994.

Kathiriya, I. S., & Srivastava, D. (2000). Left-right asymmetry and cardiac looping: Implications for cardiac development and congenital heart disease. *American Journal of Medical Genetics - Seminars in Medical Genetics*, *97*(4), 271–279.

Kawasumi, A., Nakamura, T., Iwai, N., Yashiro, K., Saijoh, Y., Belo, J. A., Shiratori, H., & Hamada, H. (2011). Left-right asymmetry in the level of active Nodal protein produced in the node is translated into left-right asymmetry in the lateral plate of mouse embryos. *Developmental Biology*, *353*(2), 321–330.

Kelly, R. G., Buckingham, M. E., & Moorman, A. F. (2014). Heart fields and cardiac morphogenesis. *Cold Spring Harbor Perspectives in Medicine*, *4*(10).

Khalifa, E. A., Tucker, M. J., & Hunt, P. (1992). Cruciate thinning of the zona pellucida for more successful enhancement of blastocyst hatching in the mouse. *Human Reproduction (Oxford, England)*, *7*(4), 532–6.

Kokkinopoulos, I., Ishida, H., Saba, R., Coppen, S., Suzuki, K., & Yashiro, K. (2016). Cardiomyocyte differentiation from mouse embryonic stem cells using a simple and defined protocol. *Developmental Dynamics*, *245*(2), 157–165.

Kosaki, K., Bassi, M. T., Kosaki, R., Lewin, M., Belmont, J., Schauer, G., & Casey, B. (1999). Characterization and mutation analysis of human LEFTY A and LEFTY B, homologues of murine genes implicated in left-right axis development. *American Journal of Human Genetics*, *64*(3), 712–21.

Kurosawa, H. (2007). Methods for inducing embryoid body formation: in vitro differentiation system of embryonic stem cells. *Journal of Bioscience and Bioengineering*, *103*(5), 389–398.

Lian, X., Zhang, J., Azarin, S. M., Zhu, K., Hazeltine, L. B., Bao, X., Hsiao, C., Kamp, T. J., & Palecek, S. P. (2013). Directed cardiomyocyte differentiation from human pluripotent stem cells by modulating Wnt/beta-catenin signaling under fully defined conditions. *Nat Protoc*, *8*(1), 162–175.

Lindsley, R. C., Gill, J. G., Murphy, T. L., Langer, E. M., Cai, M., Mashayekhi, M., … Murphy, K. M. (2008). Mesp1 coordinately regulates cardiovascular fate restriction and epithelial-mesenchymal transition in differentiating ESCs. *Cell Stem Cell*, *3*(1), 55–68.

Llames, S., García-Pérez, E., Meana, Á., Larcher, F., & del Río, M. (2015). Feeder Layer Cell Actions and Applications. *Tissue Engineering Part B: Reviews*, *21*(4), 345–353.

Logan, M., Pagán-Westphal, S. M., Smith, D. M., Paganessi, L., & Tabin, C. J. (1998). The transcription factor pitx2 mediates situs-specific morphogenesis in response to left-right asymmetric signals. *Cell*, *94*(3), 307–317.

Ma, Y., Gu, J., Li, C., Wei, X., Tang, F., Shi, G., … Jin, Y. (2012). Human foreskin fibroblast produces interleukin-6 to support derivation and self-renewal of mouse embryonic stem cells. *Stem Cell*

Research & Therapy, *3*(4), 29.

Maître, J.-L., & Heisenberg, C.-P. (2013). Three Functions of Cadherins in Cell Adhesion. *Current Biology*, *23*(14), R626–R633.

Mali, P., Yang, L., Esvelt, K. M., Aach, J., Guell, M., DiCarlo, J. E., … Church, G. M. (2013). RNA-Guided Human Genome Engineering via Cas9 Prashant. *Science*, *339*(6121), 823–826.

Maltsev, V. A., Rohwedel, J., Hescheler, J., & Wobus, A. M. (1993). Embryonic stem cells differentiate in vitro into cardiomyocytes representing sinusnodal, atrial and ventricular cell types. *Mechanisms of Development*, *44*(1), 41–50.

Marikawa, Y., & Alarcón, V. B. (2009). Establishment of trophectoderm and inner cell mass lineages in the mouse embryo. *Molecular Reproduction and Development*, *76*(11), 1019–1032.

Marques, S., Borges, A. C., Silva, A. C., Freitas, S., Cordenonsi, M., & Belo, J. A. (2004). The activity of the Nodal antagonist Cerl-2 in the mouse node is required for correct L/R body axis. *Genes and Development*, *18*(19), 2342–2347.

Martí, M., Mulero, L., Pardo, C., Morera, C., Carrió, M., Laricchia-Robbio, L., Esteban, C. R., & Izpisua Belmonte, J. C. (2013). Characterization of pluripotent stem cells. *Nature Protocols*, *8*(2), 223–253.

Martin, G. R. (1981). Isolation of a pluripotent cell line from early mouse embryos cultured in medium conditioned by teratocarcinoma stem cells. *Proceedings of the National Academy of Sciences of the United States of America*, *78*(12), 7634–7638.

Meilhac, S. M., Lescroart, F., Blanpain, C. D., & Buckingham, M. E. (2014). Cardiac cell lineages that form the heart. *Cold Spring Harbor Perspectives in Medicine*, *4*(9), 1–14.

Meno, C., Takeuchi, J., Sakuma, R., Koshiba-Takeuchi, K., Ohishi, S., Saijoh, Y., … Hamada, H. (2001). Diffusion of Nodal Signaling Activity in the Absence of the Feedback Inhibitor Lefty2. *Developmental Cell*, *1*(1), 127–138.

Mitsui, K., Tokuzawa, Y., Itoh, H., Segawa, K., Murakami, M., Takahashi, K., … Yamanaka, S. (2003). The homeoprotein Nanog is required for maintenance of pluripotency in mouse epiblast and ES cells. *Cell*, *113*(5), 631–42.

Moretti, A., Caron, L., Nakano, A., Lam, J. T., Bernshausen, A., Chen, Y., … Chien, K. R. (2006). Multipotent Embryonic Isl1+ Progenitor Cells Lead to Cardiac, Smooth Muscle, and Endothelial Cell Diversification. *Cell*, *127*(6), 1151–1165.

Morey, L., Santanach, A., & Di Croce, L. (2015). Pluripotency and Epigenetic Factors in Mouse Embryonic Stem Cell Fate Regulation. *Molecular and Cellular Biology*, *35*(16), 2716–28.

Morris, S. A., Teo, R. T., Li, H., Robson, P., Glover, D. M., & Zernicka-Goetz, M. (2010). Origin and formation of the first two distinct cell types of the inner cell mass in the mouse embryo. *Proc Natl Acad Sci U S A*, *107*(14), 6364–6369.

Muthuchamy, M., Pajak, L., Howles, P., Doetschman, T., & Wieczorek, D. F. (1993). Developmental Analysis of Tropomyosin Gene Expression in Embryonic Stem Cells and Mouse Embryos. *Molecular and Cellular Biology*, *13*(6), 3311–3323.

Naghavi, M., Wang, H., Lozano, R., Davis, A., Liang, X., Zhou, M., … Temesgen, A. M. (2015). Global, regional, and national age-sex specific all-cause and cause-specific mortality for 240

causes of death, 1990-2013: A systematic analysis for the Global Burden of Disease Study 2013. *The Lancet*, *385*(9963), 117–171.

Nakamura, T., Saito, D., Kawasumi, A., Shinohara, K., Asai, Y., Takaoka, K., … Hamada, H. (2012). Fluid flow and interlinked feedback loops establish left–right asymmetric decay of Cerl2 mRNA. *Nature Communications*, *3*, 1322.

Ng, S. Y., Wong, C. K., & Tsang, S. Y. (2010). Differential gene expressions in atrial and ventricular myocytes: insights into the road of applying embryonic stem cell-derived cardiomyocytes for future therapies. *AJP: Cell Physiology*, *299*(6), C1234–C1249.

Nichols, J., Zevnik, B., Anastassiadis, K., Niwa, H., Klewe-Nebenius, D., Chambers, I., … Smith, A. (1998). Formation of pluripotent stem cells in the mammalian embryo dependes on the POU transcription factor Oct4. *Cell*, *95*(3), 379–391.

Nichols, M., Townsend, N., Scarborough, P., & Rayner, M. (2013). Cardiovascular disease in Europe: Epidemiological update. *European Heart Journal*, *34*(39), 3028–3034.

Nishii, K., Morimoto, S., Minakami, R., Miyano, Y., Hashizume, K., Ohta, M., … Shibata, Y. (2008). Targeted disruption of the cardiac troponin T gene causes sarcomere disassembly and defects in heartbeat within the early mouse embryo. *Developmental Biology*, *322*(1), 65–73.

Nishii, K., & Shibata, Y. (2006). Mode and determination of the initial contraction stage in the mouse embryo heart. *Anatomy and Embryology*, *211*(2), 95–100.

Nishikawa, S.-I., Jakt, L. M., & Era, T. (2007). Embryonic stem-cell culture as a tool for developmental cell biology. *Nature Reviews Molecular Cell Biology*, *8*(6), 502–507.

Niwa, H., Burdon, T., Chambers, I., & Smith, A. (1998). Self-renewal of pluripotent embryonic stem cells is mediated via activation of STAT3. *Genes & Development*, *12*(13), 2048–60.

Niwa, H., Miyazaki, J., & Smith, A. G. (2000). Quantitative expression of Oct-3/4 defines differentiation, dedifferentiation or self-renewal of ES cells. *Nature Genetics*, *24*(4), 372–376.

Niwa, H., Toyooka, Y., Shimosato, D., Strumpf, D., Takahashi, K., Yagi, R., & Rossant, J. (2005). Interaction between Oct3/4 and Cdx2 determines trophectoderm differentiation. *Cell*, *123*(5), 917–929.

Nolan, T., Hands, R. E., & Bustin, S. A. (2006). Quantification of mRNA using real-time RT-PCR. *Nature Protocols*, *1*(3), 1559–1582.

Pan, G., & Thomson, J. A. (2007). Nanog and transcriptional networks in embryonic stem cell pluripotency. *Cell Research*, *17*(1), 42–9.

Parikh, A., Wu, J., Blanton, R. M., & Tzanakakis, E. S. (2015). Signaling Pathways and Gene Regulatory Networks in Cardiomyocyte Differentiation. *Tissue Engineering Part B: Reviews*, *21*(4), 377–392.

Piedra, M. E., Icardo, J. M., Albajar, M., Rodriguez-Rey, J. C., & Ros, M. A. (1998). Pitx2 participates in the late phase of the pathway controlling left- right asymmetry. *Cell*, *94*(3), 319–324.

Polanco, J. C., & Koopman, P. (2007). Sry and the hesitant beginnings of male development. *Developmental Biology*, *302*(1), 13–24.

Pourquié, O. (2003). Vertebrate somitogenesis: A novel paradigm for animal segmentation? *International Journal of Developmental Biology*, *47*(7-8), 597–603.

Quelle, D. E., Ashmun, R. A., Shurtleff, S. A., Kato, J. Y., Bar-Sagi, D., Roussel, M. F., & Sherr, C. J. (1993). Overexpression of mouse D-type cyclins accelerates G1 phase in rodent fibroblasts. *Genes and Development*, *7*(8), 1559–1571.

Ramsdell, A. F. (2005). Left-right asymmetry and congenital cardiac defects: Getting to the heart of the matter in vertebrate left-right axis determination. *Developmental Biology*, *288*(1), 1–20.

Rankin, C. T., Bunton, T., Lawler, a M., & Lee, S. J. (2000). Regulation of left-right patterning in mice by growth/differentiation factor-1. *Nature Genetics*, *24*(3), 262–265.

Robbins, J., Gulick, J., Sanchez, A., Howles, P., & Doetschman, T. (1990). Mouse embryonic stem cells express the cardiac myosin heavy chain genes during development in vitro. *J Biol Chem*, *265*(20), 11905–11909.

Rodda, D. J., Chew, J. L., Lim, L. H., Loh, Y. H., Wang, B., Ng, H. H., & Robson, P. (2005). Transcriptional regulation of Nanog by OCT4 and SOX2. *Journal of Biological Chemistry*, *280*(26), 24731–24737.

Rose-John, S. (2002). GP130 stimulation and the maintenance of stem cells. *Trends in Biotechnology*, *20*(10), 417–419.

Rungarunlert, S., Techakumphu, M., Pirity, M. K., & Dinnyes, A. (2009). Embryoid body formation from embryonic and induced pluripotent stem cells: Benefits of bioreactors. *World Journal of Stem Cells*, *1*(1), 11–21.

Ryan, a K., Blumberg, B., Rodriguez-Esteban, C., Yonei-Tamura, S., Tamura, K., Tsukui, T., … Izpisúa Belmonte, J. C. (1998). Pitx2 determines left-right asymmetry of internal organs in vertebrates. *Nature*, *394*(6693), 545–551.

Saga, Y., Hata, N., Kobayashi, S., Magnuson, T., Seldin, M. F., & Taketo, M. M. (1996). MesP1: a novel basic helix-loop-helix protein expressed in the nascent mesodermal cells during mouse gastrulation. *Development (Cambridge, England)*, *122*, 2769–2778.

Salomon, D. S., Bianco, C., Ebert, A. D., Khan, N. I., De Santis, M., Normanno, N., … Persico, G. (2000). The EGF-CFC family: Novel epidermal growth factor-related proteins in development and cancer. *Endocrine-Related Cancer*, *7*(4), 199–226.

Shah, K., McCormack, C. E., & Bradbury, N. A. (2014). Do you know the sex of your cells? *AJP: Cell Physiology*, *306*(1), C3–C18.

Shen, M. M. (2007). Nodal signaling: developmental roles and regulation. *Development*, *134*(6), 1023–34.

Shi, G., & Jin, Y. (2010). Role of Oct4 in maintaining and regaining stem cell pluripotency. *Stem Cell Research & Therapy*, *1*(5), 39.

Shiraishi, I., & Ichikawa, H. (2012). Human Heterotaxy Syndrome. *Circulation Journal*, *76*(9), 2066–2075.

Shiratori, H., & Hamada, H. (2006). The left-right axis in the mouse: from origin to morphology. *Development*, *133*(11), 2095–104.

Shiratori, H., & Hamada, H. (2014). TGF-β signaling in establishing left-right asymmetry. *Seminars in Cell and Developmental Biology*, *32*, 80–84.

Smithies, O., Gregg, R. G., Boggs, S. S., Koralewski, M. A., & Kucherlapati, R. S. (1985). Insertion of DNA sequences into the human chromosomal beta-globin locus by homologous recombination. *Nature*, *317*(6034), 230–4.

Solter, D., & Knowles, B. B. (1978). Monoclonal antibody defining a stage-specific mouse embryonic antigen (SSEA-1). *Proceedings of the National Academy of Sciences of the United States of America*, *75*(11), 5565–9.

Später, D., Hansson, E. M., Zangi, L., & Chien, K. R. (2014). How to make a cardiomyocyte. *Development*, *141*(23), 4418–31.

Suckow, M., Danneman, P., & Brayton, C. (2001). *The laboratory mouse*. CRC Press LLC.

Takaoka, K., & Hamada, H. (2012). Cell fate decisions and axis determination in the early mouse embryo. *Development*, *139*(1), 3–14.

Takaoka, K., Yamamoto, M., & Hamada, H. (2011). Origin and role of distal visceral endoderm, a group of cells that determines anterior-posterior polarity of the mouse embryo. *Nature Cell Biology*, *13*(7), 743–752.

Tam, P. P. L., & Behringer, R. R. (1997). Mouse gastrulation: The formation of a mammalian body plan. *Mechanisms of Development*, *68*(1-2), 3–25.

Tamm, C., Pijuan Galitó, S., & Annerén, C. (2013). A Comparative Study of Protocols for Mouse Embryonic Stem Cell Culturing. *PLoS ONE*, *8*(12), e81156.

Tardiff, J. C., Hewett, T. E., Palmer, B. M., Olsson, C., Factor, S. M., Moore, R. L., … Leinwand, L. A. (1999). Cardiac troponin T mutations result in allele-specific phenotypes in a mouse model for hypertrophic cardiomyopathy. *Journal of Clinical Investigation*, *104*(4), 469–481.

Thomas, K. R., Folger, K. R., & Capecchi, M. R. (1986). High frequency targeting of genes to specific sites in the mammalian genome. *Cell*, *44*(3), 419–428.

Townsend, N., Wilson, L., Bhatnagar, P., Wickramasinghe, K., Rayner, M., & Nichols, M. (2016). Cardiovascular disease in Europe: epidemiological update 2016. European Heart Journal, 37(42), 3232-3245.

Waldo, K. L., Hutson, M. R., Ward, C. C., Zdanowicz, M., Stadt, H. A., Kumiski, D., … & Kirby, M. L. (2005). Secondary heart field contributes myocardium and smooth muscle to the arterial pole of the developing heart. *Developmental Biology*, *281*(1), 78–90.

Waterston, R. H., Lindblad-Toh, K., Birney, E., Rogers, J., Abril, J. F., Agarwal, P., … & Lander, E. S. (2002). Initial sequencing and comparative analysis of the mouse genome. *Nature*, *420*(6915), 520–562.

Weitzer, G. (2006). Embryonic stem cell-derived embryoid bodies: an in vitro model of eutherian pregastrulation development and early gastrulation. *Handbook of Experimental Pharmacology*, 174, 21-51.

Williams, R. L., Hilton, D. J., Pease, S., Willson, T. a, Stewart, C. L., Gearing, D. P., … & Gough, N. M. (1988). Myeloid leukaemia inhibitory factor maintains the developmental potential of embryonic stem cells. *Nature*, *336*(6200), 684–687.

Wobus, A. M., Wallukat, G., & Hescheler, J. (1991). Pluripotent mouse embryonic stem cells are able to differentiate into cardiomyocytes expressing chronotropic responses to adrenergic and

cholinergic agents and Ca2+ channel blockers. *Differentiation*, *48*(3), 173–182.

Xin, M., Olson, E. N., & Bassel-Duby, R. (2013). Mending broken hearts: cardiac development as a basis for adult heart regeneration and repair. *Nature Publishing Group*, *14*(8), 529–541.

Yacoub, M. H., & Terrovitis, J. (2013). CADUCEUS, SCIPIO, ALCADIA: Cell therapy trials using cardiac-derived cells for patients with post myocardial infarction LV dysfunction, still evolving. *Global Cardiology Science and Practice*, *2013*(1), 3.

Yeo, C. Y., & Whitman, M. (2001). Nodal signals to Smads through Cripto-dependent and Cripto-independent mechanisms. *Molecular Cell*, *7*(5), 949–957.

Ying, Q.-L., Wray, J., Nichols, J., Batlle-Morera, L., Doble, B., Woodgett, J., … & Smith, A. (2008). The ground state of embryonic stem cell self-renewal. *Nature*, *453*(May), 519–23.

Yoshida, K., Chambers, I., Nichols, J., Smith, A., Saito, M., Yasukawa, K., … & Kishimoto, T. (1994). Maintenance of the pluripotential phenotype of embryonic stem cells through direct activation of gp130 signalling pathways. *Mechanisms of Development*, *45*(2), 163–171.

Yoshioka, H., Meno, C., Koshiba, K., Sugihara, M., Itoh, H., Ishimaru, Y., … & Noji, S. (1998). Pitx2, a bicoid-type homeobox gene, is involved in a lefty-signaling pathway in determination of left-right asymmetry. *Cell*, *94*(3), 299–305.

Zhao, S., Nichols, J., Smith, A. G., & Li, M. (2004). SoxB transcription factors specify neuroectodermal lineage choice in ES cells. *Molecular and Cellular Neuroscience*, *27*(3), 332–342.

Appendix

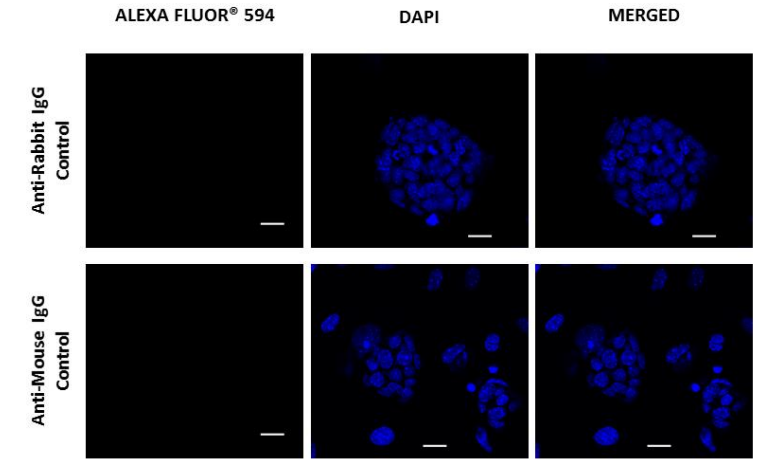

Figure A1: Control staining of the secondary antibodies used during the immunofluorescence microscopy for pluripotency markers. Images were taken in a sequence mode and the same confocal microscope settings were used for the corresponding first and second antibodies pair. Scale bars: 20 µm**.**

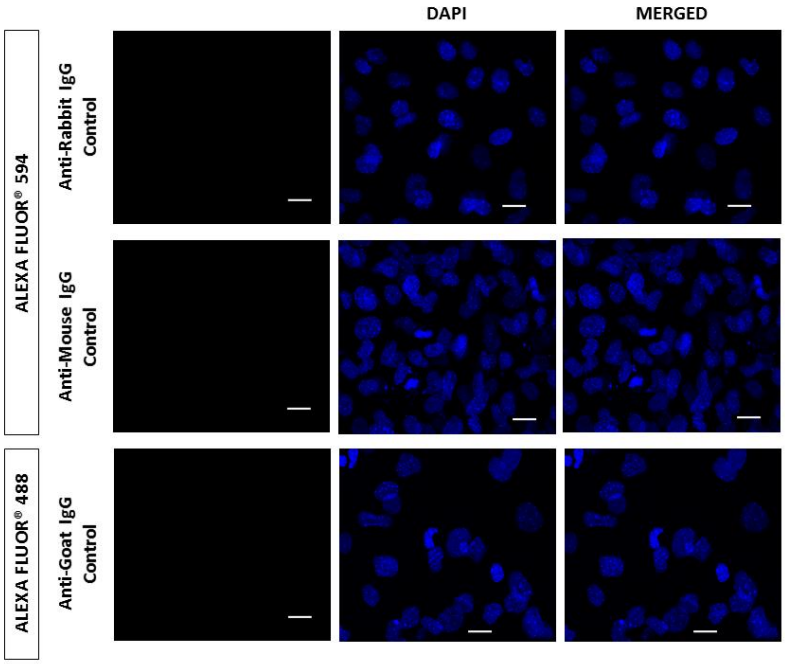

Figure A1: Control staining of the secondary antibodies used during the immunofluorescence microscopy for germ layer markers. Images were taken in a sequence mode and the same confocal microscope settings were used for the corresponding first and second antibodies pair. Scale bars: 20 µm**.**